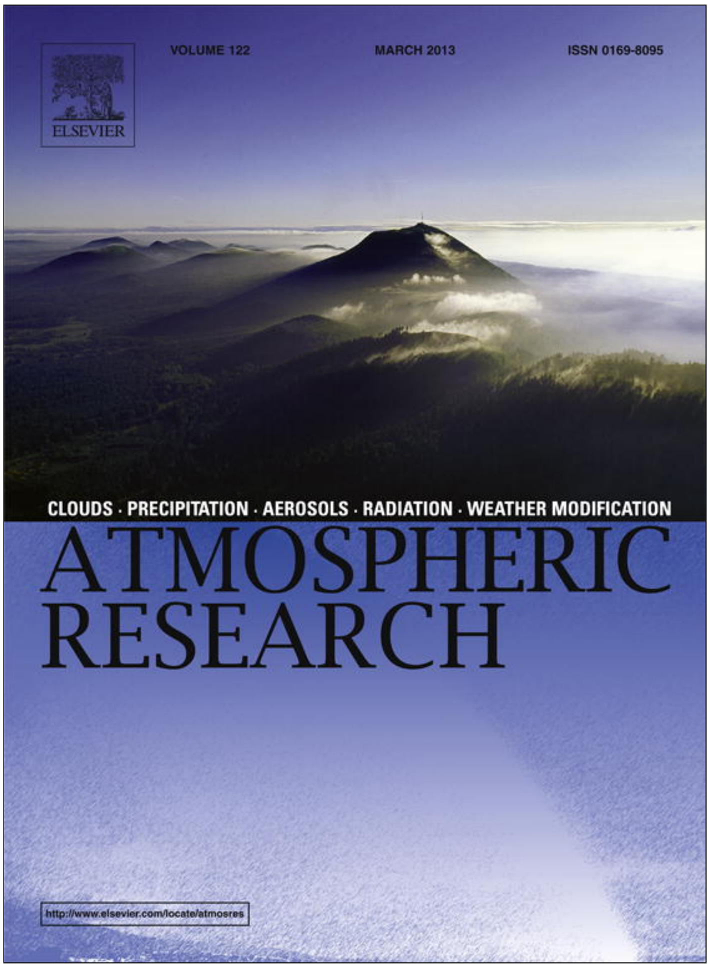
VOLUME 122
MARCH 2013
ISSN 0169-8095
ELSEVIER
CLOUDS · PRECIPITATION · AEROSOLS · RADIATION · WEATHER MODIFICATION
ATMOSPHERIC RESEARCH
http://www.elsevier.com/locate/atmosres

Atmospheric Research 122 (2013) 486–503

Contents lists available at SciVerse ScienceDirect

Atmospheric Research

journal homepage: www.elsevier.com/locate/atmos

# Mesoscale modeling of smoke transport over the Southeast Asian Maritime Continent: Interplay of sea breeze, trade wind, typhoon, and topography

Jun Wang [a,*], Cui Ge [a,f], Zhifeng Yang [a], Edward J. Hyer [b], Jeffrey S. Reid [b], Boon-Ning Chew [c], Mastura Mahmud [d], Yongxin Zhang [e], Meigen Zhang [f]

[a] Department of Earth and Atmospheric Sciences, University of Nebraska — Lincoln, NE, USA
[b] Marine Meteorology Division, Naval Research Lab, Monterey, CA, USA
[c] Centre for Remote Imaging, Sensing and Processing, National University of Singapore, Singapore
[d] Earth Observation Centre, Universiti Kebangsaan Malaysia, Selangor, Malaysia
[e] Research Applications Laboratory, National Center for Atmospheric Research, CO, USA
[f] State Key Laboratory of Atmospheric Boundary Layer Physics and Atmospheric Chemistry, Institute of Atmospheric Physics, Chinese Academy of Sciences, Beijing, China

ARTICLE INFO

*Article history:*
Received 5 September 2011
Received in revised form 19 December 2011
Accepted 12 May 2012

*Keywords:*
Southeast Asian Maritime Continent
Smoke particles
Sea breeze
Trade wind
Typhoon

ABSTRACT

The online-coupled Weather Research and Forecasting model with Chemistry (WRFchem) is used to simulate the transport of smoke particles over the Southeast Asian Maritime Continent during September–October 2006. In this period, dry conditions associated with the moderate El Niño event caused the largest regional biomass burning outbreak since 1997. Smoke emission in WRFchem is specified according to the Fire Locating and Modeling of Burning Emissions (FLAMBE) database derived from Moderate Resolution Imaging Spectroradiometer (MODIS) fire products. The modeled smoke transport pathway is found to be consistent with the MODIS true color images and measured mass concentration of surface $PM_{10}$ (particulate matter with diameter less than 10 μm). The interplay of sea/land breezes, typhoons and storms over the subtropical western Pacific Ocean, trade winds, and topographic effects, can be clearly seen in the model simulation. The most severe smoke events in 1–5 October 2006 are found to be associated with the meteorological responses to the typhoon Xangsane (#18) over the western subtropical Pacific Ocean, which moved smoke from Sumatra eastward in the lower troposphere (below 700 hPa), forming smoke layers mixed with and above the boundary layer clouds over Borneo. In contrast, the second largest week-long smoke transport event of 15–18 October 2006 was associated with the seasonal monsoonal transition period, during which smoke plumes were wide spread over the 5°S–5°N zone as a result of (a) the near surface divergence coupled with the 700 hPa bifurcation of wind (flowing both to the west and to the east), and (b) the near-surface southeasterly and easterly winds along the equator transporting smoke from Borneo to Sumatra and Peninsular Malaysia. Analysis of data from the Cloud-Aerosol Lidar with Orthogonal Polarisation (CALIOP) shows that smoke particles in October 2006 were primarily located within 3.5 km above the surface. Smoke particles contributed roughly half of the total aerosol extinction retrieved by CALIOP. Results suggest that the smoke injection height in the model should be set lower than the 2–5 km commonly used in transport simulations; smoke release at ~0.8 km instead of 2 km above surface gives a consistently better match to CALIOP observations. Numerical experiments further show that the Titiwangsa Mountains in Malaysia Peninsula and Tama Abu Mountains in Borneo have significant impacts on smoke transport and the surface air quality in the vicinity.

Published by Elsevier B.V.

* Corresponding author at: 303 Bessey Hall, Lincoln, NE, 68588, USA. Tel.: +1 402 472 3597.
*E-mail address:* jwang7@unl.edu (J. Wang).

0169-8095/$ – see front matter. Published by Elsevier B.V.
doi:10.1016/j.atmosres.2012.05.009

## 1. Introduction

The impacts of biomass burning (or smoke) aerosols on climate, through scattering and absorbing of radiation and through aerosol-cloud interaction, have been studied extensively in the past decades (e.g., IPCC, 2007). At regional scales, tropical biomass burning is often used as a means to remove crop residue, clear land for shifting cultivation, and to permanently convert forests and peatlands into agricultural areas. It is one of the largest sources of anthropogenic aerosols and trace gases in the global atmosphere (Crutzen et al., 1979; Crutzen and Andreae, 1990; van der Werf et al., 2008). Burning in tropical regions tends to have a clear seasonal cycle regulated by the movement of Intertropical Convergence Zone (ITCZ) (Giglio et al., 2006), such as Africa (Swap et al., 2003), South America (Kaufman et al., 1998), and Central America (Wang et al., 2006). The radiative forcing of smoke particles is the strongest and often can be clearly observed from either ground or satellite measurements with minimal contamination by clouds during the dry season (e.g., April–June in the northern hemisphere and August–October in the southern hemisphere).

However, the seasonality of biomass burning in the Southeast Asian Maritime Continent (MC, 10°S–10°N, 90°E–150°E), including islands of Malaysia and Indonesia, is atypical because of the following factors: (a) the "dry" season in MC (August–October) is usually associated with a considerable amount of precipitation due to the interplay of the ITCZ and the monsoon, and the separation of wet from dry seasons is only valid in the relative sense usually with ~50% difference in precipitation (Chang et al., 2005; Reid et al., 2011); (b) significant off-season burning can occur, especially during January and February when ITCZ is at its furthest south position(Reid et al., 2011); (c) besides ITCZ and monsoon systems, other multi-scale meteorological systems ranging from El Niño Southern Oscillation, Indian Ocean Dipole, the Madden Julian Oscillation, tropical cyclones and sea breeze can all affect the timing of biomass burning, increasing intra-annual and interannual variability(Field and Shen, 2008; Field et al., 2009; Reid et al., 2011); and (d) both modeling and remote sensing of smoke transport can be challenging due to the persistent and high cloud cover and generally difficult observability of sources (Reid et al., 2013).

This paper presents one of a series of studies in preparation for the 7 Southeast Asian Studies (7SEAS) field campaign including a planned intensive period in 2012 with objectives including the study of the smoke radiative effects over MC (Reid et al., 2013; also 7SEAS white paper at http://7-seas.gsfc.nasa.gov/). The focus of this paper is to combine the model simulations, ground-based and satellite observations to study smoke transport pathways over MC at higher resolutions than previous studies. Emphasis is on simulating the vertical distribution of smoke, a key determinant of both the smoke direct radiative effect (both above clouds and in clear-sky conditions) and the smoke indirect effect on clouds.

This study concerns the smoke events during September–October 2006 when a moderate El Niño event caused the largest observed biomass burning activity in MC since 1997 (van der Werf et al., 2008; Reid et al., 2011). The high fire signal, combined with the quantity and quality of satellite observations from the NASA A-Train, makes this fire season a natural case study for studying smoke in the MC. Ott et al. (2010) used the NASA's GEOS5 AGCM(Atmospheric General Circulation Model) in which the fire emission is specified based upon the Global Fire Emissions Database version 2 (GFEDv2) inventory (Randerson et al., 2005) to investigate the impact of 2006 MC biomass burning aerosols on the atmospheric lapse rate (an enhancement of 0.5–0.8 k/day in lower troposphere around MC) and the associated feedbacks on water vapor, clouds, and atmospheric transport of CO. However, the focus in Ott et al. (2010) is more on the smoke radiative feedback at the continental and seasonal scale due to the coarse model spatial resolution (1°×1.25°) of GEOS5 AGCM and temporal resolution (monthly) of GFED smoke emission. Thampi et al. (2009) showed from their AVHRR retrievals that the 2006 MC fire events resulted in significant enhancement of aerosol optical thickness over the Indian oceans, and from CALIOP observations, they found that the smoke particles were primarily located within 3 km above the surface, which is consistent with Tosca et al. (2011) that used both MISR data and CALIOP data to study the vertical profile of aerosol plumes. Hyer and Chew (2010) evaluated the Navy Aerosol Analysis and Prediction System (NAAPS) global model simulation of the smoke during the 2006 MC biomass burning season, and they found that NAAPS-simulated smoke particles, even with a model resolution of 1°, could explain 50% of observed variability of 24-h averages of $PM_{10}$ at 29 out of 54 stations in Singapore and Malaysia, in part likely due to the hourly smoke emission inventory the NAAPS model used.

These previous studies used global models at relatively coarse resolution for modeling the transport and radiative effects of aerosols over MC. This model resolution (1°×1° at best and often coarser than 2°×2°) may not be sufficient to capture fine-scale but important meteorological effects such as sea breeze, or topographic effects, on the distribution of smoke particles. Indeed, as described by Reid et al. (2011), fire activity tends to occur in shorter events that covary with localized meteorological features that may not be well captured in a global scale model. The current study uses an online-coupled regional Weather Research and Forecasting model with Chemistry (WRF-Chem) with two principal goals: (a) to evaluate the performance of a regional CTM (Chemical Transport Model) in simulating the smoke transport in a complex meteorological environment such as MC, and (b) to examine the aerosol direct and indirect radiative forcing and feedbacks on the atmospheric heating rate, as well as the sensitivity of the forcing to the aerosol optical and physical properties. This paper will only focus on (a), while results from (b) will be presented in a separate paper. Our emphasis is on the simulation of the aerosol vertical profile because it strongly affects the aerosol radiative feedback on surface temperature and atmospheric lapse rate (Wang and Christopher, 2006). We describe the data and model configuration respectively in Sections 2 and 3, present and evaluate the model results in Section 4, and summarize the major findings in Section 5.

## 2. Data and area of study

The area of interest in this study is the Maritime Continent in Southeast Asia (Fig. 1). The data sets used in this study

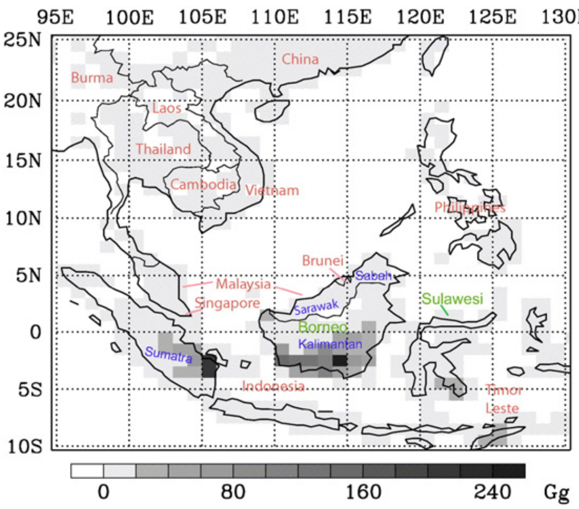


**Fig. 1.** WRFchem fine-grid model domain overlaid with the map of gray-coded total smoke emission (1 Gg = $10^9$ g) from FLAMBE database during 1 September to 31 October 2006. Names of relevant countries are denoted in red color, islands in green color, and regions in blue color.

include (1) hourly smoke emissions from FLAMBE polar-orbiting satellite (MODIS-based) database, (2) ground-based $PM_{10}$ observations, and (3) satellite observations from CALIOP and MODIS.

### 2.1. FLAMBE emission

The Fire Locating and Modeling of Burning Emissions (FLAMBE) (http://www.nrlmry.navy.mil/flambe/) polar-orbiting satellite database is used in this study to specify the smoke emissions as a function of space and time. Specifically, FLAMBE algorithm estimates the smoke emission using the method originally proposed by Seiler and Crutzen (1980), in which the emission of smoke particles is parameterized as a function of the total amount of fuel mass available for combustion, the combustion factor, the average mass faction of carbon, the total area burned, and the emission factor (Reid et al., 2009). The emission factors that FLAMBE uses are based on the review of Reid et al. (2005), while the biomass characteristics are based on the land surface database as described in Reid et al. (2009). The unique feature of FLAMBE is its use of the information content from the satellite-based fire products for the near-real-time estimation of hourly fire emission.

Over the eastern hemisphere and high-latitude regions where near real-time geostationary satellite-based fire product is not yet fully tested, FLAMBE uses the fire products from MODIS instruments aboard Terra and Aqua satellites. Fire detection data are thus obtained 3–4 times per day in tropical and mid-latitude regions and more frequently in the high latitude regions (Justice et al., 2002; Giglio et al., 2003; Reid et al., 2009). FLAMBE assumes a fire area of 62.5 ha (0.625 $km^2$) for each fire pixel that MODIS detects (Reid et al., 2009). Even in the clear sky days, 3–4 observations per day from polar-orbiting satellites are still insufficient to characterize the life time of the fires. Consequently, assumptions must be made about the lifetime of a satellite-detected fire in order to apply the FLAMBE emission in a chemistry transport model that requires the smoke emission rate as a function of time. FLAMBE assigns MODIS fires a duration of 24 h from the hour of first detection, with a diurnal cycle applied so that roughly 90% of smoke emissions are released during daylight hours (Reid et al., 2004). For the WRFchem simulations in this study, we distribute the FLAMBE estimated smoke emission for each fire equally within 6 h in the WRFchem. This gives the same timing of smoke release as is currently used in the NAAPS model (Reid et al., 2009).

The distribution of total smoke particles emitted during the time period of 1 September–31 October 2006 shows that the major emission sources are located at central Kalimantan region (2.5S, 115E) and Sumatra (2.5S, 105E) region (Fig. 1). Qualitatively, the smoke emissions hotspots correspond to the first EOF of dominant MC emissions identified by Field and Shen (2008), and is largely associated with peatland burning (Reid et al., 2012). In total, FLAMBE estimate gives ~3.48 Tg emission of smoke particles during September and October of 2006, which is much lower than 26.07 Tg of smoke emission for the same two months in 1997 as estimated by Davison et al. (2004) using fire products from Along-Track Scanning Radiometer (ATSR) and Advanced Very High Resolution Radiometer (AVHRR). This is in part consistent with Logan et al. (2008) who showed the CO emission in 1997 in our study region is much larger (or a factor of 3–4) than that in 2006, but also likely reflecting that FLAMBE emission generally has a low bias by a factor of 2 (Wang et al., 2006; Reid et al., 2009; Fisher et al., 2010). For this study, FLAMBE smoke emission values are multiplied by 2 before input in WRFchem.

### 2.2. $PM_{10}$ observations

The Malaysian Department of Environment (DOE) operates a network of 49 air quality monitoring stations in Malaysia. 35 of those stations are located in Peninsular Malaysia, which is separated from the Indonesian island of Sumatra by the Straits of Malacca. The other 14 stations are situated in East Malaysia, north of the Indonesian territory of Kalimantan in Borneo. More information on measurements, site locations and the daily Air Pollutant Index are available online (Department of Environment Malaysia, 2010: http://www.doe.gov.my/portal/air-air-quality/air-quality/).

The air quality monitoring stations are positioned strategically in industrial, urban and sub-urban areas as well as along roadsides to monitor the ambient air quality. The concentrations of major criteria pollutants such as sulfur dioxide, nitrogen oxide, carbon monoxide, ozone and $PM_{10}$ are measured daily. The $PM_{10}$ measurements used in this study are obtained via the beta attenuation method (National Environment Agency, 2006).

### 2.3. Satellite observations

For the purpose of model evaluation, MODIS true-color images, MODIS fire products (Justice et al., 2002), and aerosol vertical profiles from CALIOP (Winker et al., 2010) are used in this study. MODIS aerosol product (Levy et al., 2007) is not used for model evaluation because the high cloud cover in the study region strongly reduces the number of valid retrievals. MODIS is a radiometer with 36 channels covering various atmospheric window and water absorption channels in 0.4–15 μm. MODIS detects fire pixels or IR "hot spots" at 1 km resolution using two

4 μm channels with saturation temperatures of 500 K and 335 K respectively and one 11 μm channel with a saturation temperature of 400 K (Kaufman et al., 2003). Only MODIS fire level-2 products are used in this study.

The Cloud-Aerosol Lidar with Orthogonal Polarisation (CALIOP) instrument, aboard the Cloud-Aerosol Lidar and Infrared Pathfinder Satellite Observation (CALIPSO) satellite launched in 2006, is a two-wavelength (532 and 1064 nm), polarization-sensitive (at 532 nm) lidar that measures atmospheric backscattering with a single-shot vertical and horizontal resolution of 30 and 333 m, respectively. The lidar ratio is needed to convert the backscattering to the total extinction, and the CALIPSO aerosol algorithm selects a "best-match" lidar ratio from a series of steps: (1) feature mask based upon the depolarization ratio and the backscattering coefficient measured by CALIOP to separate clouds from aerosols, and to differentiate layers of non-spherical dust particles from layers of spherical particles; (2) based upon geolocation and season of CALIPSO observation as well as the feature mask in step (1), the type and the lidar ratio of aerosols are selected from a look-up table that is generated from a cluster analysis of AERONET data and in situ observations, respectively (Omar et al., 2005; Winker et al., 2009, 2010). To fulfill feature finding and layer classification requirements, the current CALIOP level-2 algorithm yields an aerosol layer product at a horizontal resolution of 5 km and vertical resolution of 60 m under 20 km. In this study, the quality control flag in CALIOP level-2 product is used to ensure that the best quality layered AOD at 532 nm are used in the evaluation of WRFchem simulations.

## 3. Model description

### 3.1. WRFchem model and assimilation of FLAMBE emission

The WRFchem model (Grell et al., 2005; Fast et al., 2006), version 3.1, is used in this study. WRFchem not only has all the capability that WRF has for weather forecast and regional climate studies, but also can simulate the aerosol life cycle and aerosol-cloud-radiation interactions, as well as the gas-phase chemistry (Grell et al., 2005; Fast et al., 2006). With its nested grid-capability, the WRFchem model has been used in several field campaigns to study aerosol processes because the simulated quantities can be more easily compared to a wide range of in-situ and remote sensing data collected at different temporal and spatial resolutions. Fast et al. (2006) showed that the predicted shortwave radiation during the 2000 Texas Air Quality Study was closer to the observed values when the impact of aerosols on radiation was included. Barnard et al. (2010) showed that the WRFchem simulated single scattering albedo (SSA) was too high compared to observations in Mexico City, but the agreement improved when using the observed aerosol mass, composition, and size distribution to drive the aerosol optical component in WRFchem. Zhao et al. (2010) showed that the WRFchem simulated aerosol optical depth associated with dust over West Africa compared reasonably well with MISR satellite data. Simulated vertical profiles of heating rates by WRFchem also agreed reasonably well with field measurements near the surface, although larger differences in the mid-troposphere were noted, possibly due to the underestimation of the contribution of biomass burning aerosols (Zhao et al., 2010).

The specification of smoke emission rate in WRFchem follows Wang et al. (2006). The smoke emission rate within a grid cell of area A ($m^2$) is calculated as:

$$\left(\frac{\partial C}{\partial t}\right)_{emission} = \frac{\sum_{j} F_j}{A \bullet H \bullet t}$$

where j represents jth fire within that grid; F is the smoke emission flux (kg); H is the injection height (m), and the assumption is that the smoke particles are well mixed in all model layers below this height. Since hourly smoke emission is used, $\Delta t$ is set to 1 h. It is worth noting that since the lifetime of a fire is assumed to be 6 h, for the same MODIS-detected fire pixel at the over passing hour t, its emission rate is held constant between t and t + 5 h.

It is a common practice in aerosol transport models to uniformly distribute the smoke aerosols within H so that the buoyancy caused by the heat from fires can be taken into account (Wang et al., 2006). However, there is no consensus on the method of defining H in the model. Prior studies suggest various values of H ranging from 2 km in global CTMs (Liousse et al., 1996; Forster et al., 2001; Davison et al., 2004; Reid et al., 2009) to 5–8 km in regional simulations of smoke from intensive Canadian fires (Westphal and Toon, 1991; Colarco et al., 2004). The height reached by smoke aerosols and trace gases near the source has been shown to strongly affect transport outcomes and smoke observability with remote sensing systems (Hyer et al., 2007; Leung et al., 2007). Recently, observations from MISR aerosol plume height have revealed that smoke particles are not uniformly distributed within the boundary layer (Kahn et al., 2007; Val Martin et al., 2010), and that the incorporation of a 1D plume rise model in the model grids shows the potential to improve the model simulations of smoke transport (Guan et al., 2008; Freitas et al., 2007; Sessions et al., 2011). However, depending on the time difference between the MISR observations and the fire ignition, the aerosol plume height as seen by MISR may not be the same as the smoke injection height needed in the model (Kahn et al., 2007). The rise of a smoke plume depends on both ambient atmospheric profile and the heat released from the burning over the fire area (not model grid area). The latter quantity is not readily available from the observations, although can be related to the MODIS-derived fire radiative power (Kahn et al., 2007; Ichoku and Kaufman, 2005). For the sake of simplicity, this study distributes the emitted smoke particles uniformly within the injection height H. A series of model simulations using different H (see Section 4.4) showed that a value of 0.8 km gives the best agreement with CALIOP observations. This result also agrees with the recent findings of Tosca et al. (2011) using MISR and CALIPSO. As shown in Section 4, the 2-km injection height used by Davison et al. (2004) for the simulation of smoke transport over the Indonesian region in 1997 is indeed too high.

### 3.2. Model configuration

A nested grid configuration is used in this study, with a fine grid of 112 × 97 points and 27 km grid spacing covering

Southeast Asia, nested within a coarse grid with 100 × 127 grid points and 81 km grid spacing (Fig. 1). Both horizontal grids use 27 vertical levels in the terrain-following hydrostatic pressure coordinates system unequally spaced from the ground to approximately 20 km, with approximately 9 layers concentrated in the lowest 2 km of the atmosphere to resolve the planetary boundary layer. The lowest model layer is approximately 20 m above the surface. The 1° × 1° National Center for Environmental Prediction (NCEP) Final Analysis (FNL) data at 0000, 0600, 1200 and 1800 UTC are used for initializing and specifying the temporally evolving lateral boundary conditions. The microphysics and cumulus parameterization used here are the WRF Single-moment 5-class (WSM5) scheme (Hong et al., 2004) and Grell ensemble cumulus scheme (Grell and Devenyi, 2002), respectively. The boundary layer scheme used was the Yonsei University (YSU) scheme (Hong et al., 2006). The land surface model used was the Noah LSM that includes the unified NCEP/NCAR/AFWA scheme with soil temperature and moisture in four layers, fractional snow cover, and frozen soil physics. The time-varying SST, sea ice, vegetation fraction, and albedo were updated from the NCEP reanalysis data during the model simulation.

The simulations of aerosol processes use the Second Generation Regional Acid Deposition Model (RADM2) (Stockwell et al., 1990) and the Modal Aerosol Dynamics Model for Europe with Secondary Organic Aerosol Model (MADE/SORGAM) (Ackermann et al., 1998; Schell et al., 2001). The shortwave radiative scheme uses the two-stream multi-band Goddard model (Chou et al., 1998) with ozone climatology, while at infrared wavelengths, the RRTM scheme (Mlawer et al., 1997) is used. Since the focus of this paper is the transport of smoke particles and no biogenetic and anthropogenic emission database that has the native resolution suitable to be used for the meso-scale modeling in MC, the background (including anthropogenic) aerosol and the transport of aerosol particles from outside the model boundary, as well as the aerosol radiative feedback are not included in the model simulation.

We treat all smoke emissions as $PM_{2.5}$ emission in WRFchem, and consider the simulations with injection height at 0.8 km as the baseline simulation, with other simulations used for sensitivity analysis in Section 4. All numerical simulations are initiated at 00 UTC on August 20, 2006 and ended at 00 UTC on November 2, 2006. However, only data during 1 September–31 October 2006 are analyzed.

## 4. Results and analysis

The $PM_{10}$ mass measurements at various stations during 1 September–31 October 2006 indicate that the air quality in Singapore and Malaysia including Malaysian Borneo (Fig. 2a–i) was severely degraded by the smoke events. The $PM_{10}$ mass variations shown in Fig. 2 illustrate that major smoke events occurred in late September and the first three weeks of October, during which the $PM_{10}$ mass concentrations at various stations were 10%–100% higher than the corresponding averages (horizontal sold line in each panel of Fig. 2). Although there were quite a few sporadic events of smoke transport from time to time, two major smoke transport events occurred during 2–12 October and 14–23 October over Peninsular Malaysia (e.g., the gray-shaded time periods in Fig. 2a–d), and three time periods of smoke events during 24–30 September, 2–8 October, and 11–18 October, over Borneo island (Fig. 2e–h).

The transport pathway between the smoke source region and the downwind region can be traced from the time series of daily $PM_{10}$ data at different ground stations. In general, the increase of $PM_{10}$ due to the smoke transport is larger at the southern stations than at northern stations (which is visible from the dotted lines across different panels in Fig. 2),

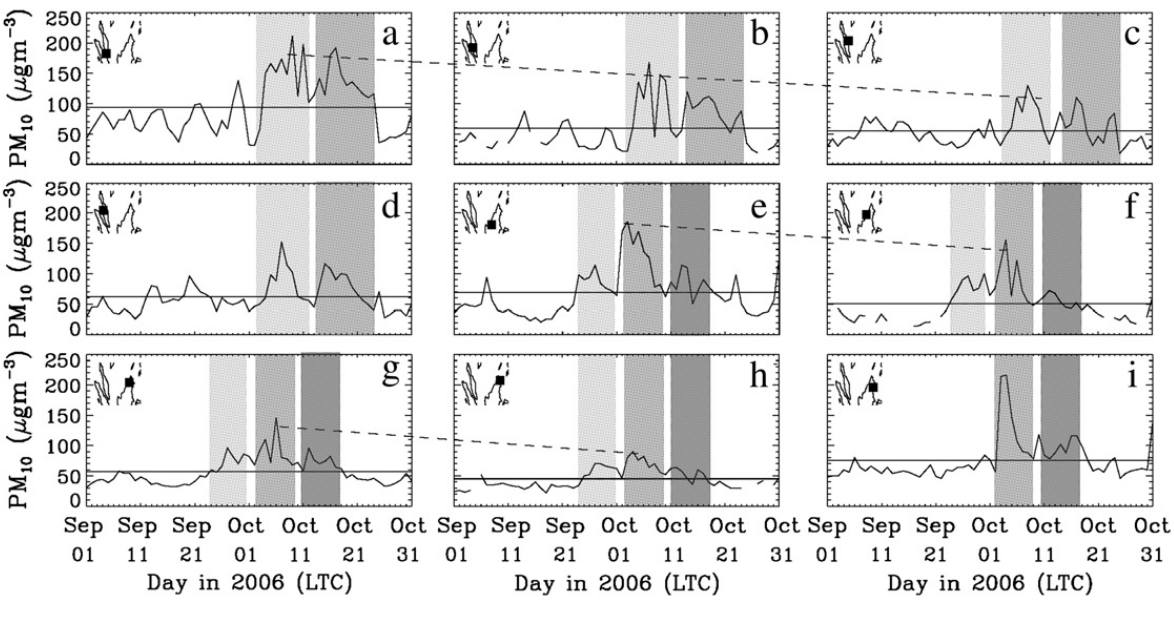


**Fig. 2.** Time series of daily-averaged $PM_{10}$ mass concentration ($\mu g\ m^{-3}$) in various ground-based stations during September–October, 2006. The inset map on the upper right of each panel shows the location of the station (denoted as solid square), while the horizontal line shows the two-month average of $PM_{10}$ mass concentration at that station. The shaded background in different time intervals highlights the time frames of week-long major smoke events, and dotted lines connecting the peak of $PM_{10}$ mass concentration in various panels illustrate the south-to-north gradient of surface aerosol mass concentration during the smoke transport events (see text for details).

reflecting in part the diffusion and deposition during the smoke transport.

Since 1–9 October 2006 is the time period when surface air quality over both Peninsular Malaysia and Borneo Island was most severely degraded by the smoke (Fig. 2), this time period is analyzed in detail. We describe our analysis in the following two sections respectively focusing on 1–2 October in Section 4.1, and 3–9 October in Section 4.2. As it will be shown, the contrast between these two cases shows differences in smoke transport pathways that explain why over Borneo, the peak of $PM_{10}$ concentration occurred on 2–3 October (Fig. 2e–i), while over Peninsular Malaysia, the peak event was 5–6 October (Fig. 2a–c). In Section 4.3, we present the analysis of the second largest week-long (11–18 October) smoke event (Fig. 2). The comparison of this event with the first event (in Sections 4.1 and 4.2) shows not only differences in the lower tropospheric transport that signals the shift from the summer monsoon to the winter monsoon, but also features of the vertical distribution of aerosols that are further studied in detail in Section 4.4. A quantitative assessment of overall performance of WRFchem simulation is presented in Section 4.5 together with the summary of the common smoke transport mechanisms during the two months of our study period. Finally, a sensitivity analysis of the topographic effect on smoke transport is conducted in Section 4.6.

### *4.1. Smoke transport in 1–2 October 2006: typhoon effect*

MODIS true color images (Fig. 3a–b) show that there were fires over both central Kalimantan and east Sumatra during 30 September–1 October 2006. However, during the same period, the ground-based observations (color dots in Fig. 3g–h) showed almost no increase of $PM_{10}$ over stations in Peninsular Malaysia (Fig. 2a–c) before 3 October, and a sharp (a factor of 2) increase of $PM_{10}$ over many stations along the coast of Sarawak did not start until 2 October (Fig. 2e–h). This interesting timeline of smoke transport can be explained by meteorology that, as discussed below, is also related to the propagation of fires in central Kalimantan and eastern Sumatra.

Typically during the summer monsoon, winds in the South China Sea are southwesterly, and draw smoke from Sumatra and Borneo up into the monsoonal trough which runs from northern Vietnam diagonally toward New Guinea (Reid et al., 2011). Reid et al. notes that smoke production and transport along this pathway are enhanced by two climatologically collinear features. First, drying associated with the later phases of the Madden Julian Oscillation (4–8) enhance both smoke production in the MC and transport in the South China Sea. At the same time, tropical cyclone activity in the northern South China Sea tends to be enhanced in the middle and early late MJO phases. Large scale subsidence around tropical cyclones can further retard convection in the region. These dynamics were strong factors in this region's meteorology in 2006. The category 3 Typhoon Xangsane (#18, according to the Automated Tropical Cyclone System) was over the western tropical Pacific (15°N, 115°E) on 30 September (Fig. 3a) and landed on Vietnam on 1 October 2006 (Fig. 3b). As a result, the stations along the coast of Malaysian Borneo were primarily affected by enhanced westerly or southwesterly winds that carried the smoke particles from Sumatra (Fig. 3g–h), and were not affected by the smoke particles generated from the southeast (or over central Kalimantan). Indeed, in areas right north to the coast of Sarawak, the surface wind was in the west and/or southwest direction on 30 September (Fig. 3g), converging with the southeasterly smoke-polluted winds from Kalimantan. On 1 October, to compensate for the strong low-level dynamical convergence of the typhoon centered at Cambodia (Fig. 3b), Kalimantan and Sumatran regions must have dynamic divergence near the surface (as manifested by wind vectors in Fig. 3h), which led to the downdraft and dryness that in turn favored fire propagation (red spots on Fig. 3b–c).

While the wind pattern at the surface is complex, the winds at 700 hPa are more consistent (Fig. 3m–o). Under the influence of the anti-clockwise wind flow around the periphery of the typhoon in the 10°–20°N zone, the westerly winds in 0°–10°N zone were strong and efficiently transported the smoke from Sumatra to Kalimantan and Malaysian Borneo, usually above or within the boundary-layer clouds as seen from MODIS images (Fig. 3a–b) and CALIOP observations (Fig. 4c). The transported smoke particles are generally confined within the lower troposphere (as seen from CALIOP observations in Fig. 4c for 1 October), likely due to the downdraft over Borneo. Baseline model simulations with injection height at 0.8 km (Fig. 4b) generally agree with the CALIOP observation, but simulations with injection height at 2 km (as commonly used in the literature) result in enhancement of smoke particles in the middle troposphere above 4 km that is not observed in the satellite data (Fig. 4a).

After the landfall on 1 October 2006, the Typhoon intensity decreased dramatically during 2–4 October 2006 as the MODIS true color images in these days (Fig. 3c–e) indicated the continuous decrease of cloud cover Vietnam and Cambodia. One interesting feature we found after 1 October is the opposite phase in the temporal evolution of biomass burning activities between Central Kalimantan and eastern Sumatra: when Central Kalimantan shows a large number of MODIS fire counts (such as on 3 October, Fig. 3d), Sumatra shows fewer or zero fire counts, and vice versa (such as on 4 October, Fig. 3e). This kind of seesaw pattern lasts during 2–8 October until both regions showed little fire events on 9 October (Fig. 3f). This could be real, associated with the general length scale of tropical convection (we can see differences in cloud cover in the RGB images). However this may also in part be due to orbit considerations from MODIS, with higher fire sensitivity at nadir relative to the limb.

As the Typhoon weakened into a low pressure system over Thailand on 2 October 2006 (Fig. 3c), the subsequent change in meteorology over the MC was the stronger component of southerly wind at the surface over Borneo, which helped to transport smoke from central Kalimantan to the stations along the coast of Malaysian Borneo, leading to a sharp increase of $PM_{10}$ over those stations (Fig. 2e–h and color dots on Fig. 3i). On 2 October, smoke particles reached the northern tip of Borneo, and stations over Brunei and Sabah showed their highest $PM_{10}$ values in the two months that we studied (these stations are in red in Fig. 3i instead of yellow as in Fig. 3h). At 700 hPa, however, the wind pattern was similar to the previous day; the strong westerly wind

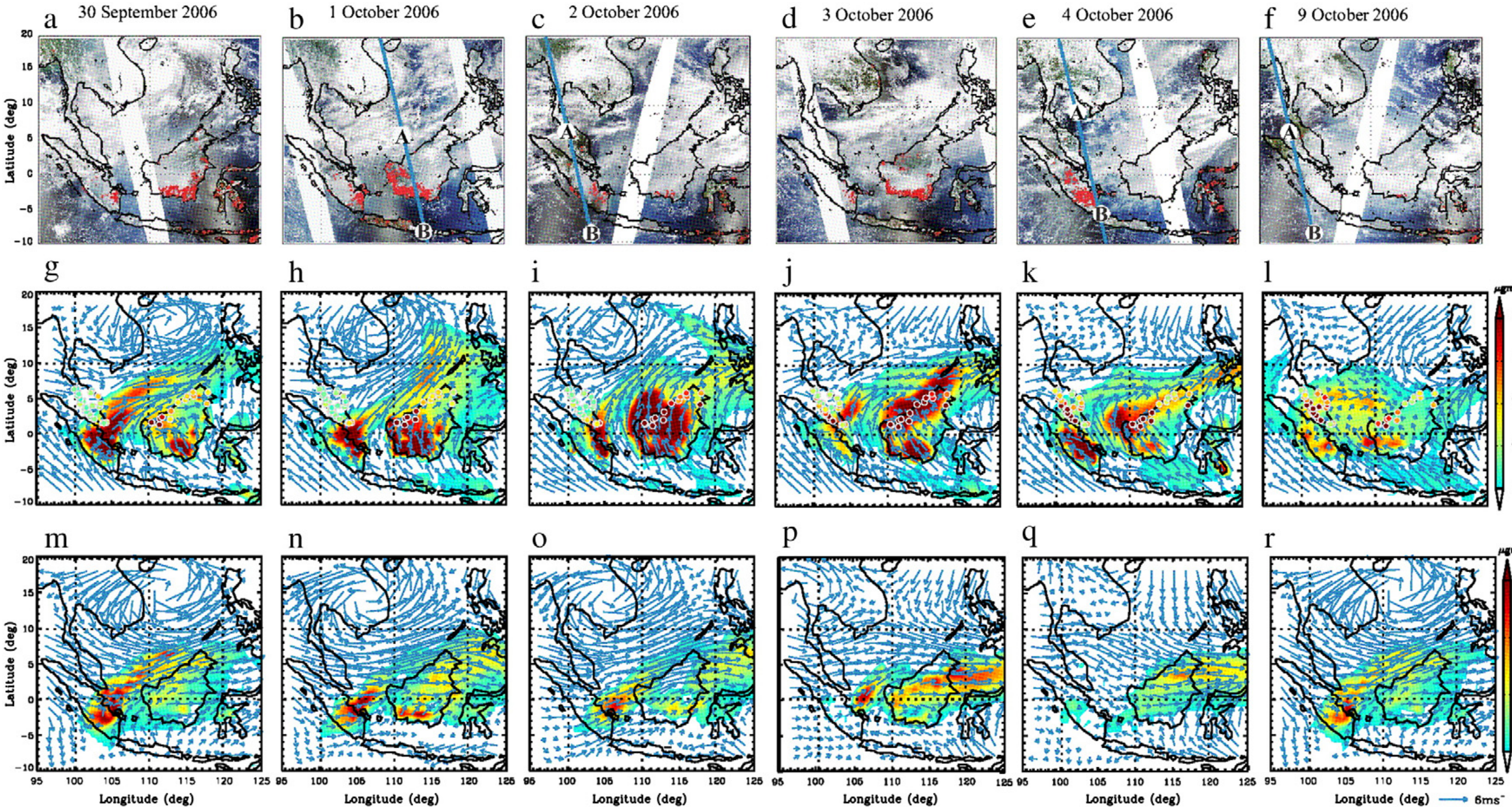


**Fig. 3.** (a–f) MODIS three-band color overlay images (red, band 1; green, band 4; and blue, band 3) from Terra and Aqua satellites for days in 30 September–4 October and 9 October 2006. Red dots indicate the location of fires detected by MODIS. Blue solid lines indicate the ground track of CALIPSO satellite; letters A and B bracket the part of the ground track where the CALIOP data is compared against WRFchem results in Fig. 4. (g–l) Modeled dry smoke concentration (μg $m^{-3}$) near the surface at 06:00 UTC (or 13:00 local time) at days respectively corresponding to the (a–f). Solid dots show the locations of different $PM_{10}$ observation sites and are color-coded on the same color scheme as that used for the color-filled contour of modeled smoke concentration (e.g., the legend on the right side of panel (l)). Also overlaid is the wind speed near the surface. (m–r) Same as (g–l) but for smoke particle concentration and wind vector at 700 hPa. No ground-based observations are shown on (m–r).

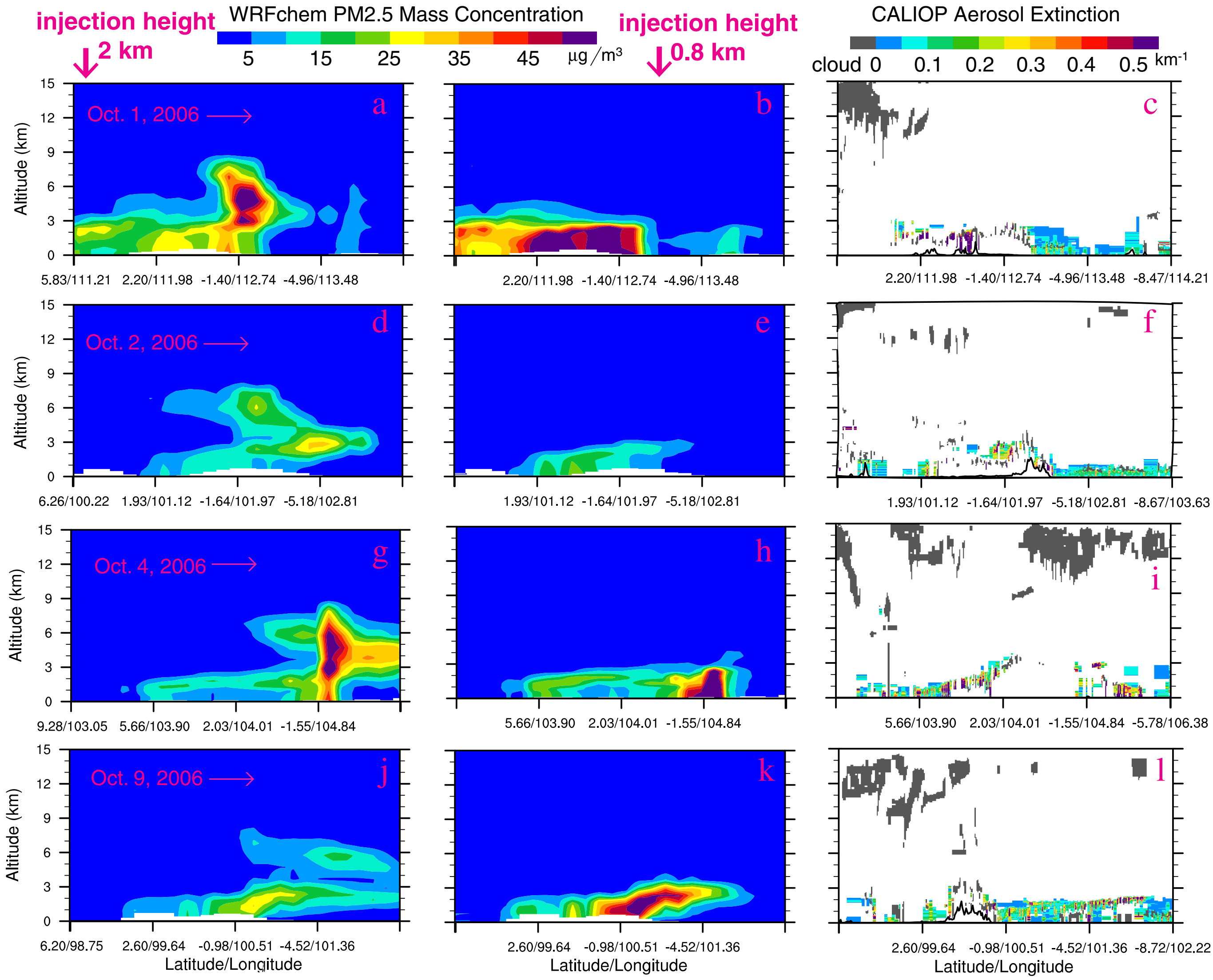


**Fig. 4.** Inter-comparison of CALIOP-derived vertical profile of aerosol extinction coefficient (third column) with the WRFchem simulated vertical profile of smoke concentration along the corresponding CALIPSO ground track (left column and middle column) on 1 (first row from the top), 2 (second row), 4 (third row), and 9 (bottom row) of October 2006. The model results in the first column are from the simulation that set the smoke injection height at 2 km, while in the second column the smoke injection height is set at 0.8 km in the model (e.g., baseline simulation). The ground tracks of CALIOP data in (c), (f), (i) and (l) are shown as AB lines respectively in Fig. 3b, c, e, and f.

continuously transported smoke particles from Sumatra to Borneo. CALIOP data again shows that smoke particles were confined within 1–2 km above the 0.5–1 km boundary layer clouds (Fig. 4f).

Although the Typhoon made the meteorology during 1–2 October special, the synoptic conditions we discussed in this section is by no means singular (Reid et al., 2011). During the two months of our study period, several cases can be seen from satellite images and model simulations that the downdraft and clear skies (and so fires) over the equatorial region in central Kalimantan are often associated with the low pressure systems (sometime storms) over the subtropical western Pacific Ocean (figures not shown).

### *4.2. Smoke transport on 3–9 October 2006: sea breeze and trade winds*

After 2 October, $PM_{10}$ concentration over west coast of Borneo, particularly near Brunei and Sabah, progressively decreased and remained low after 4 October (Fig. 3k–l). The model simulations (Fig. 3j–l) show that the concentration of smoke particles remained high over the stations along the western part of the Sarawak coastline on 4 October, which is consistent with ground-based $PM_{10}$ observations (color dots in Fig. 3j–l). Detailed examination of the wind pattern on 3–4 October 2006 revealed surface divergence along the coast of Sarawak, Brunei, and Sabah, and surface convergence slightly north of the coast line (Fig. 3j–k). This divergence/convergence pattern can be understood as the effect of sea breeze. During the day (when MODIS true color images are collected, and also the time for model simulations plotted in Fig. 3), the in-shore sea breeze counteracts the southeasterly trade wind over the land, and this counteraction effect is relatively distinct in the north part of the coast of Borneo where the trade winds are weaker. During the afternoon time when the sea breeze is the strongest, the wind can change direction from southeast to northwest over the northwest coast of Borneo. Consequently, this weak northwesterly wind acts together with stronger westerly or southwesterly flow over the ocean to form a divergence zone, while colliding with the inland southerly trade winds to form a convergence zone, both of which are clearly demonstrated in Fig. 3j–l.

The effect of sea breeze, as discussed here, for stabilizing the air mass of smoke particles along the northwest coast of Borneo is also repeatedly observed in our 2-month WRFchem simulation. To illustrate this effect, we compute the anomaly in 2-month averages of surface wind in September–October 2006 as a function of local times employing two steps. Firstly, the 2-month averaged wind vector at each hour (hereafter $\vec{V_J}$, where $J$ is the subscript for hour and ranges from 1 to 24) is computed, from which the 24-hour mean wind vector $\vec{V}_{MEAN}$ $\left(=\sum_{J=1}^{J=24}\vec{V_J}/24\right)$ is estimated. Secondly, the anomalies of wind vector at each hour $\left(\vec{V_J}-\vec{V}_{MEAN}\right)$ are calculated and shown in Fig. 5 at every 4 h from 02:00 to 22:00 local time. While the model grid resolution of 27 km usually is too coarse to simulate the sea breeze along the coast line, Fig. 5 clearly shows that the sea breeze around MC is strong. The onshore northwestern sea breeze weakens the southwestern offshore winds at ~5°–10°N in the morning (Fig. 5a–c), and sometimes can completely shift the wind direction toward land in the late afternoon (Fig. 5c–d), leading to the convergences of smoke particles respectively over the Malaysian Borneo coast in daytime (Fig. 5b–d) and over the Malaysian Borneo coastal water in night time (Fig. 5e–f). In contrast, during the evening, the offshore land breeze enhances the southwestern trade winds, moving smoke off of the coast. As a result, smoke particles are repeatedly transported inland and seaward on a daily basis until they are scavenged by local precipitation. Mahmud (2009) numerically simulated the effect of sea breeze on the smoke transport in 1997.

Opposite to the change of surface smoke mass concentration over Borneo was the increase of $PM_{10}$ over Peninsular Malaysia during 3–4 October and the persistence of high $PM_{10}$ in that region until 9 October, which can be seen from the change of colors at stations over west Malaysia and Singapore in Fig. 3j–l as well as the time series of $PM_{10}$ in Fig. 2a–c. This can be explained by the shift of wind direction in the northeast parts of Sumatra and Peninsular Malaysia and their nearby oceans (i.e., the equatorial wind centered around 105 E) from southwest during 30 September–2 October (Fig. 3g–i) to south and later southeasterly wind on 3–9 October 2006 (Fig. 3j–l). This wind direction change together with the occurrence of fires over Sumatra (Fig. 3d–f) enabled the continuous northwestward transport of smoke particles from Sumatra to Singapore and Malaysia.

At 700 hPa, westerly winds dominated between 0° and 10°N during 3–9 October, and so smoke particles from Sumatra were often transported over Borneo (Fig. 3p–r). As consistently shown by the CALIOP data (Fig. 4i and l) and baseline model simulations (Fig. 4h and k), the smoke particles were confined in the lowest 4 km layer above the surface, similar to the 1–2 October case in Section 4.1.

In summary, while significant changes in surface wind pattern can occur on daily or sometimes hourly basis (such as sea breeze) as shown in Fig. 3g–l, the 700 hPa wind during 1–9 October appeared to be dominated by the westerly wind

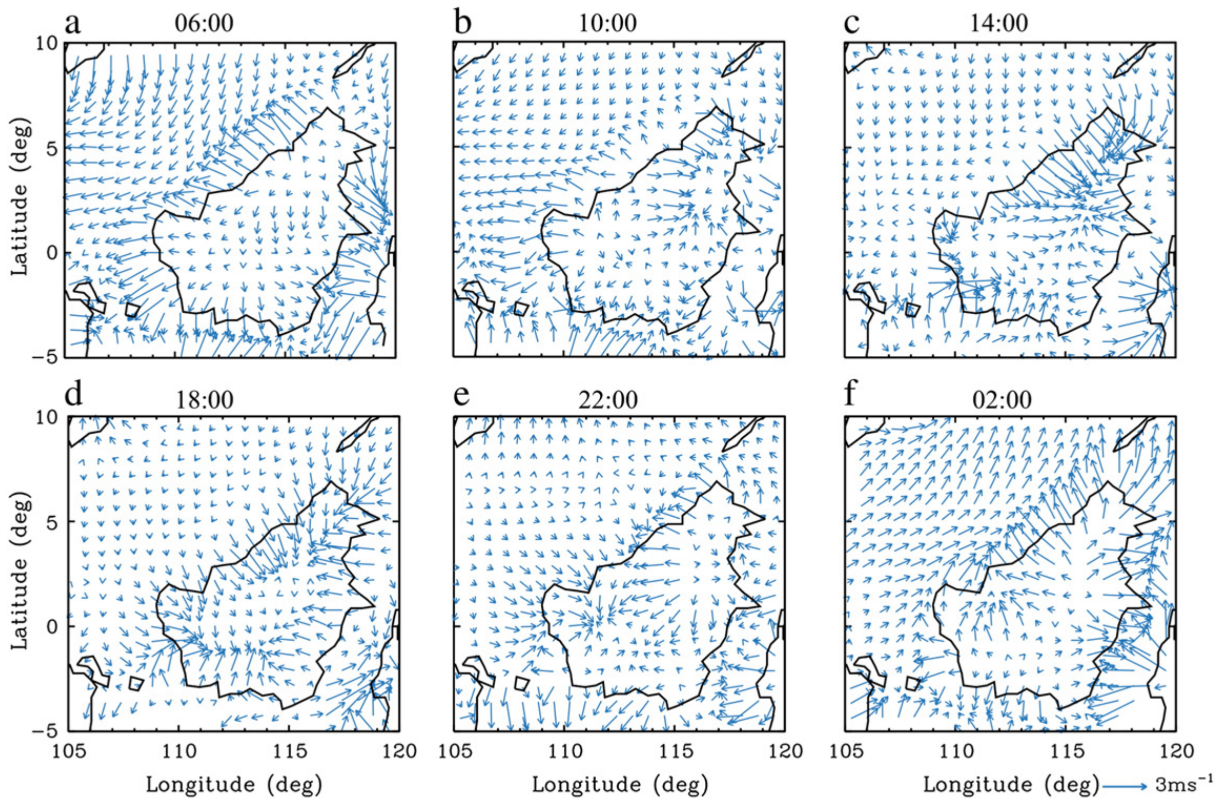


**Fig. 5.** Anomaly in 2-month averages of surface wind in September–October 2006 as a function of local times respectively at (a) 6:00, (b) 10:00, (c) 14:00, (d) 18:00, (e) 22:00, and (f) 2:00. See Section 4.6 for details.

that efficiently transported the smoke aerosols generated from fires in Sumatra over Peninsular Malaysia to be either above or mixed with cloud layer over Borneo (Fig. 3m–r). However, the overall low-level clock-wise circulation around Kalimantan and Malaysian Borneo indicates that the low-level divergence associated with the downdraft can efficiently trap the smoke from venting upward and transporting eastward (as shown by CALIOP data on Fig. 4c, f, i, l and baseline simulation on Fig. 4b, e, h, k). Sensitivity simulations with injection height of 2 km often show an artificially high aerosol concentration above 4 km (Fig. 4a, d, g, j).

### 4.3. Smoke transport on 11–17 October 2006: monsoonal transition and the southward movement of ITCZ

The second largest of these smoke events occurred during 11–17 October 2006 and was recorded over most ground stations (Fig. 2 and color dots in Fig. 6d–f) and also was manifested in the simulated results with a larger impact of smoke aerosols on air quality in Singapore and Peninsular Malaysia than in Malaysian Borneo (filled color contours in Fig. 6d–f). In contrast to the smoke events of 2–12 October (Fig. 3), fewer MODIS fire counts can be found over MC during 11–18 October (Fig. 6a–c), with higher concentrations of $PM_{10}$ over the northwest part of Peninsular Malaysia, and lower over Malaysian Borneo, as seen in Fig. 6d–f. During 15–17 October, the $PM_{10}$ concentration at most stations over Peninsular Malaysia is more than 100 μg m$^{-3}$. Model simulations in Fig. 6 also appear to be more consistent with the measurements of $PM_{10}$ at the ground than their counterparts in Fig. 3. One possible explanation for this is that the lower fraction of cloud cover during 15–17 October (Fig. 6a–c as compared to Fig. 3a–f) may have permitted better detection of fires for accurate estimate of smoke emission. High concentrations of smoke particles during 15–17 October were found not only over Borneo but also over the ocean to the west of Sumatra and Peninsular Malaysia (Fig. 6); these ocean areas did not see high $PM_{10}$ concentrations during 30

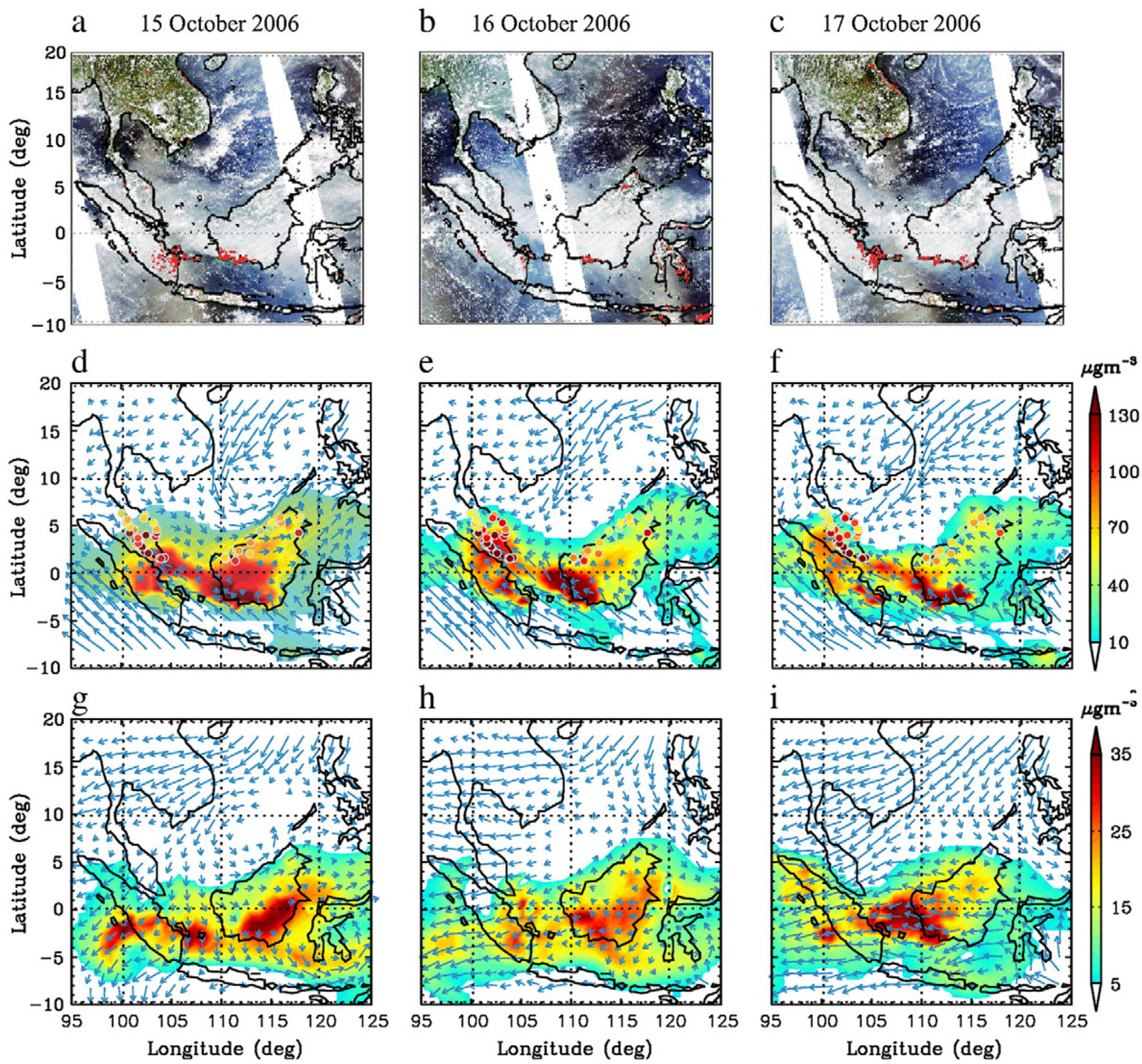


**Fig. 6.** Same as Fig. 3 but for 15, 16, and 17 of October 2006 from the left column to the right column, respectively.

September to 9 October 2010. This wide spread of smoke aerosols in 5°S–5°N zone (Fig. 6) is due to the change in meteorology associated with the fall-to-winter transitional southward movement of ITCZ.

Mid to late October is the time when the MC region begins to shift from the boreal summer to winter monsoonal position. The resultant change in wind patterns associated with movement of the ITCZ can be clearly seen in Fig. 6 during 15–16 October 2006. The westerly and southwesterly prevailing winds in the 5°N–10°N zone that were responsible for carrying smoke particles from Sumatra to Borneo (such as on 15 October 2006, Fig. 6d and g) have been replaced by easterly and northeasterly winds that transport smoke from Borneo to Peninsular Malaysia (such as on 16–17 October, Fig. 6e–f and h–i). Near the surface of 5°S–5°N zone, this shift in wind direction combined with the southeasterly trade winds south of the equator allows the continuous transport of smoke particles from Kalimantan to Sumatra and then onto Peninsular Malaysia (Fig. 6d–f), which explains why higher concentration of smoke particles (~70–100 $\mu g\ m^{-3}$) can be seen in many northern stations over Peninsular Malaysia. The convergence zone where northeasterly and southeasterly winds meet can be clearly identified over the oceans (centered around 2.5°N, 110°E) between Peninsular Malaysia and Kalimantan (Fig. 6e and f), leading to the upward movement of smoke particles. However, this upward movement is then intercepted by the bifurcation of wind (around 10°N, 110°E) at around 700 hPa, which carries smoke particles that were transported from the surface to both the east and west directions (Fig. 6g–i). At 700 hPa south of the equator, easterly winds generally prevailed and transported smoke from Kalimantan to Sumatra, and then to the Indian ocean (Fig. 5g–i), although sometimes bifurcation of low-level winds can also occur (such as at regions of $5 \pm 3$°N, $110 \pm 5$°E at 700 hPa Fig. 6g–h), spreading the smoke particles in both east and west directions. As a result of these divergences, a broad tropical belt with higher concentration of smoke particles was formed between −5°S and 5°N (Fig. 6d–i), which differs from the distribution of smoke during the first smoke event period (30 September–9 October) when smoke was mostly transported to the northeast toward the Philippines (Fig. 3g–l). However, what is in common to both smoke event periods is the well trapped smoke aerosol layers below around 700 hPa (figures similar to Fig. 4 but for 11–17 October 2006 are not shown).

The above situation demonstrates a flow pattern unique to El Niño years. As discussed in Reid et al. (2011) and Xian et al. (2012) in neutral or La Nina years, the monsoonal transition is associated with widespread precipitation over the MC which effectively ends the fire season. However, in 1997, 2004, and 2006 El Niño events (but interestingly not 2009), precipitation is not associated with the monsoonal shift, and fires can actually intensify. With the wind reversal in the South China Sea, smoke from Borneo is now transported into the more heavily populated regions of the Malay Peninsula.

### 4.4. Aerosol vertical distribution and smoke injection height

To test the robustness of our finding about aerosol vertical distribution in the two week-long smoke events in October 2006 (as described in Sections 4.1–4.3), we compute the statistics of CALIOP-based level-2 aerosol products in our study region during the entire month of October 2006 (Fig. 7a), and compare the statistics with those in other years (Fig. 7d–g). We note consistent results that aerosol loadings during October 2006 were primarily located within 3.5 km above the surface, and generally decreased with altitude (Fig. 7a). However, due to the narrow swath of CALIPSO's ground track, interpretation of CALIOP data always needs to address the issues of limited spatial coverage and the problem of detecting aerosols below and between different layers of clouds. This is particularly important in our study region where high-level cirrus clouds (shown as dark shades at 6 km or higher altitudes in Fig. 4c, f, i and l) are very frequent over much of the region (Reid et al., 2013). Indeed, if we count each atmospheric column that CALIOP level-2 aerosol product (5 km in the horizontal) covers as one data sample, we can find that the maximum frequency (normalized probability to all samples) for CALIOP to detect an aerosol-contaminated 300-m thick layer (e.g., 5 vertical bins of CALIOP level 2 data) in an atmospheric column is ~10% at the height of 0.9–1.2 km (shown in Fig. 7c as color-coded valid aerosol observation frequency). This detection frequency decreases to 5% at 2.1 km, and approaching to zero when altitude is above 4 km (Fig. 7c), which, as expected, indicates the low possibility of an aerosol layer at middle-to-upper troposphere. However, what is unexpected is that the detection frequency also decreases from 0.9 km (the 3rd bottom dark red dots in Fig. 7c) to the surface, though there should be more aerosols near the surface. This may be understandable considering the factor that the shallow boundary layer clouds in the area (~0.5 km above surface as shown in Fig. 4c, f, i, l) significantly attenuate the CALIOP lidar beam and thus limit the ability of CALIOP to measure aerosols near the surface.

Given the limitations of CALIOP coverage to compare the model with the statistics of CALIOP data we performed an analysis of WRFchem simulations along the CALIOP ground track within the nested model domain between 10°S–10°N and 95°E–125°E where most smoke particles reside. The model statistics are for all sky conditions, and are interpolated and binned at a vertical resolution of 300 m (equivalent to 5 vertical intervals in the CALIOP level-2 aerosol data); the layers where aerosols and clouds coexist are not filtered out. One can use CALIOP cloud information to filter these cases out from the analysis, but the mismatch of spatial resolution (both horizontally and vertically) between the model simulation and CALIOP poses a challenge. Nevertheless, we find that aerosol profiles simulated with smoke release from the surface to 0.8 km (Fig. 7b) are generally consistent with CALIOP data, both showing that most aerosols are located within 3.5 km, and the peak of aerosols is ~1.0 km. The model simulations with the injection height set at 2 km (red line in Fig. 7b) show a rather different picture than that of CALIOP data.

Both baseline WRFchem simulation and CALIOP statistics consistently show that there are large fluctuations of aerosol extinction within 3.5 km above the surface. CALIOP statistics (Fig. 6c) further indicate that large layer aerosol optical depth (AOD of 0.06 in a 300-m layer) can occur more than 2% of the time within 2 km; this probability (shown as frequency percentage in Fig. 7c) decreases to 1% between 2 and 4 km.

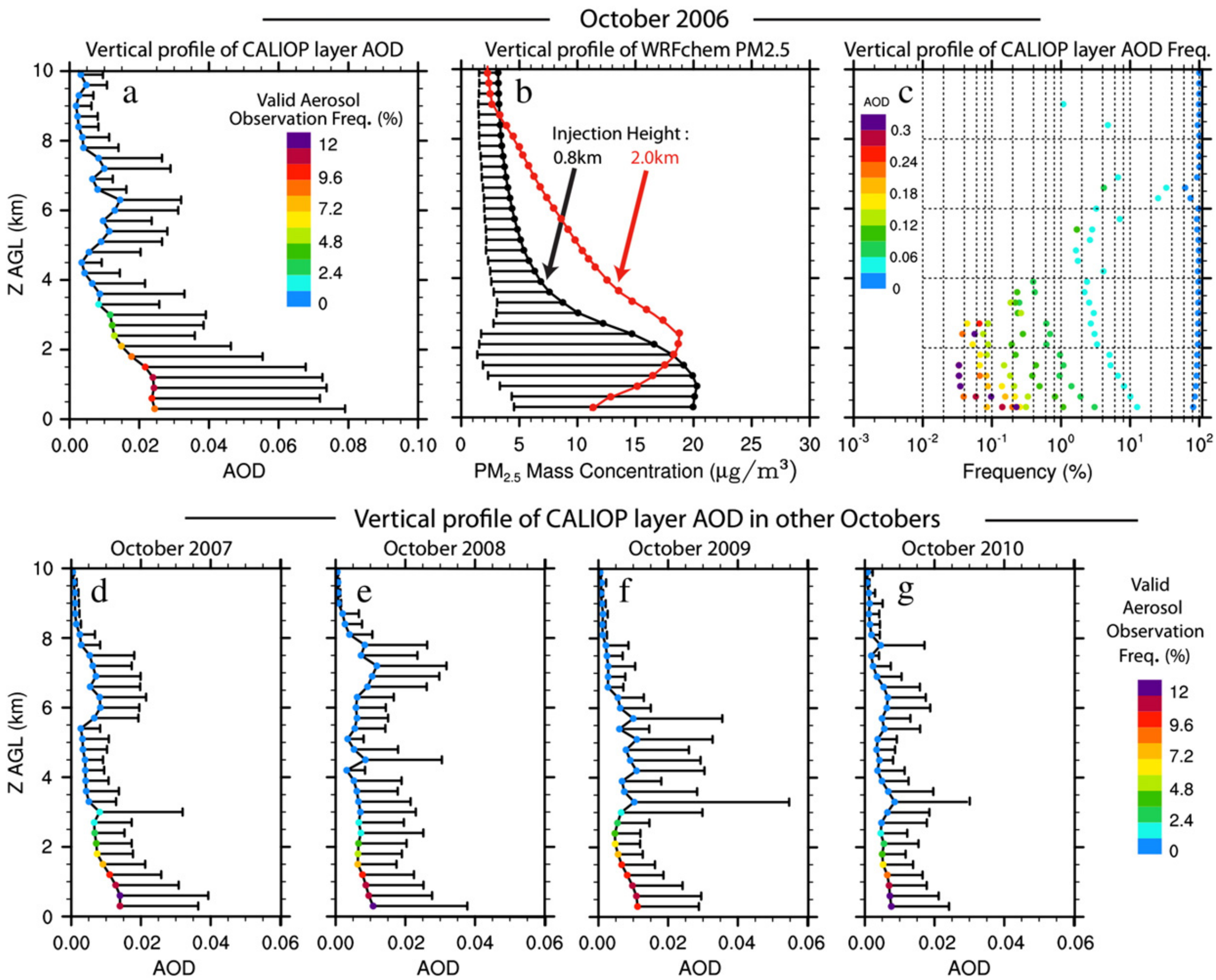


**Fig. 7.** (a) Monthly averages of CALIOP-retrieved layered (300-m thick) AOD at 0.532 μm as a function of altitude above ground level (AGL). (b) Similar as (a) but for WRFchem simulated $PM_{2.5}$ (e.g., smoke particle) mass concentration along the CALIPSO ground track. The length of the horizontal bar at each layer represents the one standard deviation for all valid aerosol optical depth (AOD) data sampled at that layer. (c) Frequency of CALIOP-derived AOD distribution at each layer. The frequency for different AOD ranges at each 300-m layer is computed based upon all the CALIOP-derived AOD values in October at the corresponding layer, and are denoted as filled circles color-coded for different AOD ranges (with interval of 0.03). (d)–(g) are the same as (a) but respectively for 2007, 2008, 2009, and 2010.

Generally, taking the study domain as a whole, we find that the probability to have larger layer AOD decreases at higher altitudes (Fig. 7c).

The aerosol detection/observation probability revealed in Fig. 6a is not unique to this study period, and is consistent with the CALIOP data in other Octobers in 2007–2010 as shown in Fig. 7d–g). The probability of observing an aerosol layer within the boundary layer from CALIOP is generally less than 10% in October over Maritime Continent due to the frequent presence of high cloud in the region. Comparison of Fig. 7a with Fig. 7d–g also shows that the October 2006 smoke event is the largest among the last 5 Octobers. Near the surface, the (300-m thick) layer AOD at 532 nm is ~0.01 averaged from 2007 to 2010 (Fig. 8a), and more than double that in 2006. Fig. 8b shows the difference in layer AOD between 2006 and averages from 2007 to 2010, from which an enhancement of smoke AOD of about ~100% in 2006 is clearly seen within 2 km (contrast between Fig. 8a and b) above the surface, providing additional support for setting smoke injection height below 2 km. Similarly, the frequency of larger values (>0.01) of (300-m) layer AOD is nearly doubled in 2006 compared to the averages in other years (Fig. 8c). Although we also find significant increase of layer AOD in 5–7 km in October 2006 (as shown in Fig. 8b), it is unclear if this anomaly is due to the cirrus cloud contamination (even though we have used the quality control flag to get the highest-confidence CALIOP aerosol data in our analysis) or in fact due to the aerosols.

### *4.5. Overall assessment of simulated smoke transport: indications of topographic effects*

Geographically, WRFchem simulations of surface $PM_{2.5}$ distribution in 2-month (September–October 2006) averages, as shown qualitatively in Fig. 9a, capture the observed south-to-north gradient (in Fig. 2) in both Malaysia and Indonesia (and a more quantitative analysis of this agreement is shown later in Fig. 10). High smoke concentrations at the surface are simulated by WRFchem in the smoke source region in the southern hemisphere, e.g., central Kalimantan and east

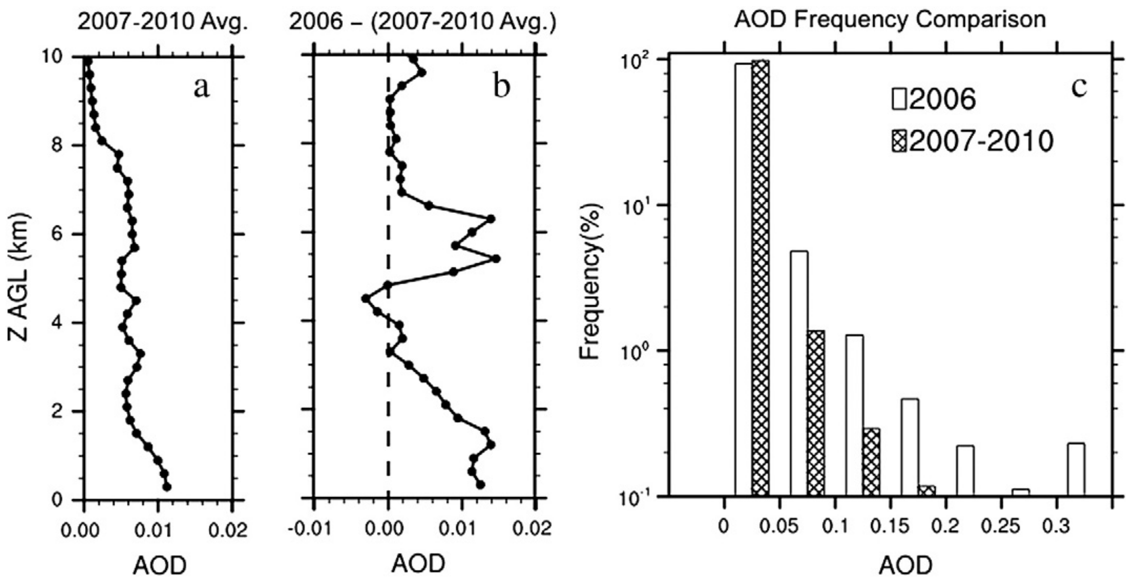


**Fig. 8.** Analysis of layer AOD based upon CALIOP data. (a) Mean of 300-m layer AOD (x-axis) at different above ground level (AGL) during 2007–2010 Octobers. (b) The difference of 300-m layer AOD (x-axis) between 2006 October and the mean of 2007–2010 Octobers at different AGLs. (c) Frequency of 300-m layer AOD within 3 km above the surface in 2006 (shown as white bars) and in 2007–2010 as whole (shown as shaded bars).

Sumatra. These air masses with high concentrations of smoke aerosol particles are then transported by the southeast trade winds across the equator (Fig. 9a). Their continuous north-westward movement in the northern hemisphere is then affected by the Coriolis force that generates a cross-isobar flow to the right, and consequently, their directions are shifted to the north (at ~5°N), and then eventually move eastward or northeastward at ~5°–10°N zone. As a result, a convergence zone at10°–15°N (in some days shown as a low pressure system centered at 15°N, 115°E) can be formed over the ocean between the westerly wind at ~10°N and the northeasterly trade wind (at ~20°N). Over the land, anticyclones or high pressure systems are consequently formed and can often be found from surface to mid-troposphere (~500 mb). These features suppress the updraft and enhance the surface (soil/biomass) dryness, with both favorable for the ignition of fires (as shown in the 1–2 October case analyzed in Section 4.1). Consistent with this conceptual model, MODIS true color images in September–October 2006 often showed that smoke aerosols can hover over Malaysian Borneo and Indonesian Kalimantan for as long as two weeks. It is worth noting that the meteorological systems shown in Fig. 9a are averages in September–October 2006. On the daily scale, the transition from sea breeze in the day time to land breeze at night time, as discussed in Section 4.2, is also interesting, especially near the Malaysian Borneo coast, the downwind from the smoke source in Kalimantan.

Quantitatively, the scatter plots of daily averages of modeled $PM_{2.5}$ and measured $PM_{10}$ during the 2 months of study period for each (of 9) stations in Fig. 2 are shown in

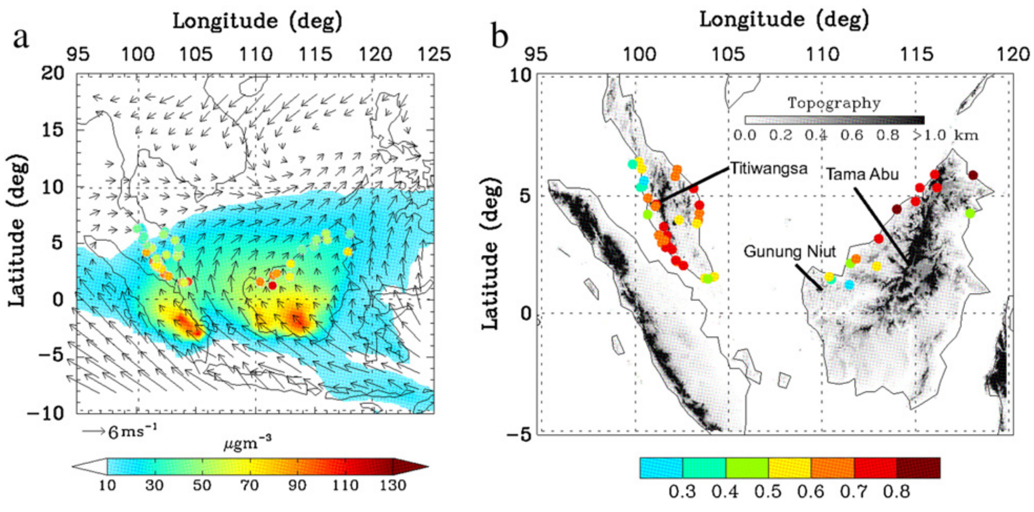


**Fig. 9.** (a) Geographical distribution of averages of WRFchem simulated surface $PM_{2.5}$ mass concentration in September–October 2006, overlaid with the corresponding averages of surface wind vector and the $PM_{10}$ mass concentration measured by the ground stations (denoted as filled-color circles). (b) Geographical distribution of linear correlation coefficients between WRFchem simulated daily surface $PM_{2.5}$ concentration and the daily surface $PM_{10}$ mass concentration measured at each ground sites (denoted as filled-color circles); also overlaid is the topography shown with colors ranging from white for elevation at sea level to black color for elevation larger than 1 km. Three mountain ranges, Titiwangsa, Tama Abu, and Gunung Niut, are also marked in the (b).

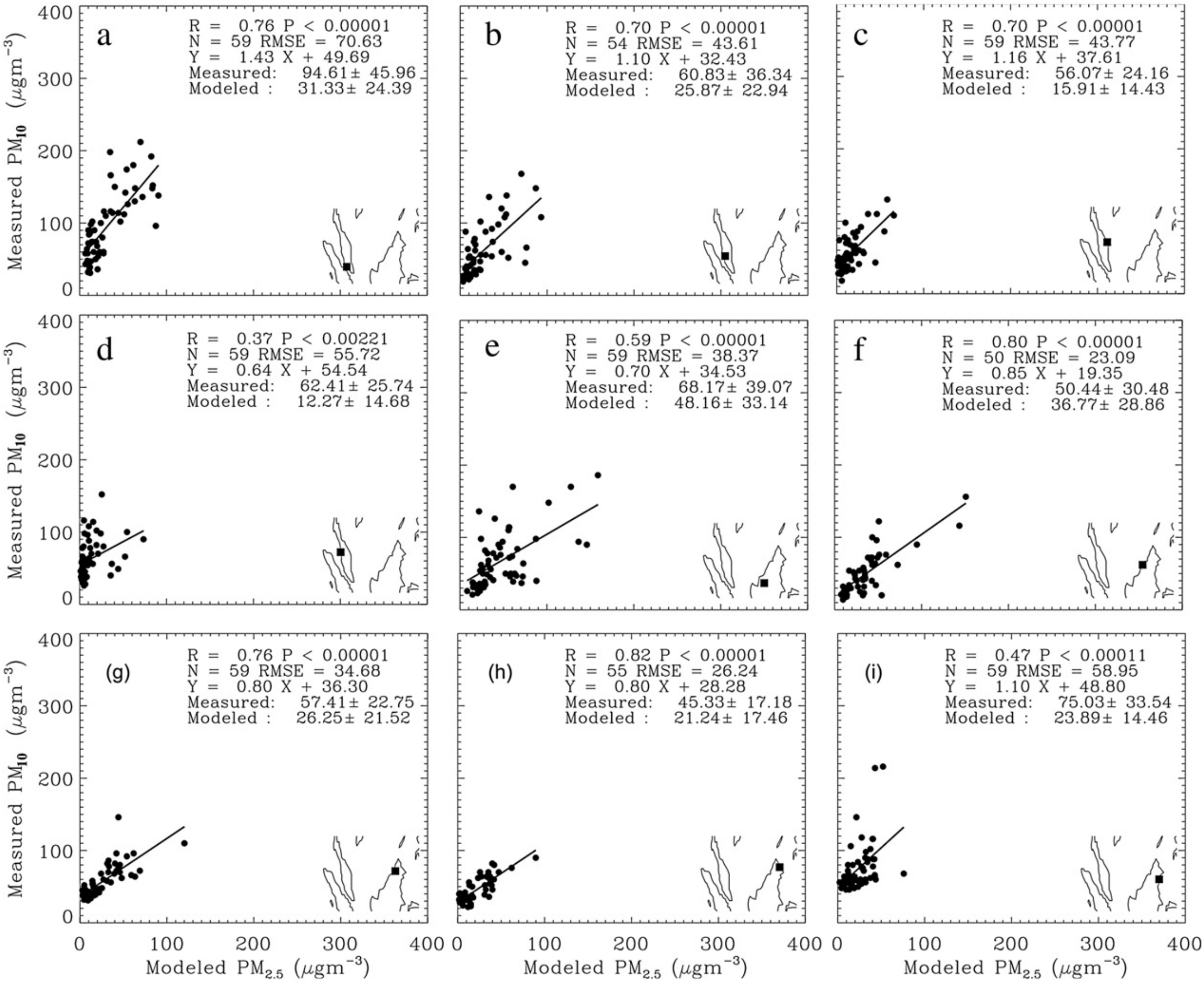


**Fig. 10.** Comparison between daily averaged WRFchem simulated smoke ($PM_{2.5}$) concentrations (x-axis) near the surface with the measured $PM_{10}$ concentration (y-axis) near the surface at different individual site (solid square in the inset map, and also corresponding to the sites showed in Fig. 2). Also shown in each panel are the correlation coefficient (R), the significance level of correlation (P, not significant when P greater than 0.05), number of comparison pairs (N), root mean square error (RMSE), and mean ± standard deviation of both modeled and measured quantities.

Fig. 10. The figure reveals that the smoke particles had a strong impact on the air quality in many downwind stations (Fig. 10a–c and e–h) where modeled $PM_{2.5}$ and measured $PM_{10}$ frequently show correlations better than 0.7 at a statistical significance level of 95%. Geographically, Fig. 8b shows the map of correlation coefficients between modeled daily $PM_{2.5}$ and measured daily $PM_{10}$ correlation for all 49 stations, which demonstrates that the modeled $PM_{2.5}$ at most stations can explain 50% or more variability in the measured $PM_{10}$. Contrast between Figs. 1 and 9b clearly indicates the high correlations between the modeled $PM_{2.5}$ and measured $PM_{10}$ are primarily located in the northwestern or north direction with respect to the smoke source region, indicating that the transport path of smoke is primarily influenced by the southeasterly low-level trade winds.

However, Fig. 9b also reveals that a few stations with low correlation (less than 0.5) are located either near the Gunung Niut Mountain between Kalimantan and Sarawak or in the northwestern foothills of the Titiwangsa Mountains over Malaysia Peninsula, suggesting a potential impact of topography on the transport of smoke. Chang et al. (2005) showed that the complex terrain has a clear impact on the distribution of precipitation in Borneo and Peninsular Malaysia, presumably due to the orographic uplifting effect. Fig. 9a clearly shows that smoke generated from the fires in Central Kalimantan region is transported toward the northwest and then moves along (or over) the western side of Tama Abu Mountain Range to the Malaysian Sarawak and Brunei coast. The Gunung Niut (centered at 1.5°N, 110°E) mountain also influences smoke transport: simulated smoke particle concentrations are reduced on the leeward side of this mountain, and correlations between simulated $PM_{2.5}$ and observed $PM_{10}$ are lower for these stations. Similarly, the intrusion of smoke particles from the east Sumatra region to the Singapore and Malaysia can be intercepted by the south–north range of Titiwangsa Mountains, and hence the smoke transport is stewed toward the north instead of reaching the west coast of the Malaysian Peninsula. Quantitatively, the significantly low measured $PM_{10}$ concentrations and also the even lower modeled smoke concentrations are found at the stations whose path to the smoke source region is intercepted by the mountains (two examples are shown in Fig. 10d and i).

### 4.6. Sensitivity experiment to topography

We conducted a numerical sensitivity experiment to support aforementioned hypothesis of the topographic effect on the smoke transport. The experiment is the same as the baseline simulation except for reducing the altitudes of 300-m and higher topography in Peninsular Malaysia and Borneo uniformly to 300 m (Fig. 11a). This reduction essentially flattens and lowers the topography of Gunung Niut mountain, Titiwangsa Mountains, and Tama Abu Mountain Range (as shown in Fig. 11a). The simulation after the reduction of topography shows, in 2-month averages, an increase of up to 8 μg m$^{-3}$ (20%–100% increase) of smoke concentration at the surface in the leeward side of the Tama Abu and Titiwangsa mountains, and a decrease of similar amount in the windward side of these mountains (Fig. 11b). This change of surface aerosol concentration can be interpreted with the help of Fig. 11b showing that the southeasterly wind along the coast of Malaysian Brunei (Sarawak, Brunei, and Sabah) is largely increased after lowering the topography. While a detailed examination of topographic effect on atmospheric dynamics and orographic clouds and precipitation warrants a separate study, we also see an increase of simulated $PM_{2.5}$ from the northern part of Peninsular

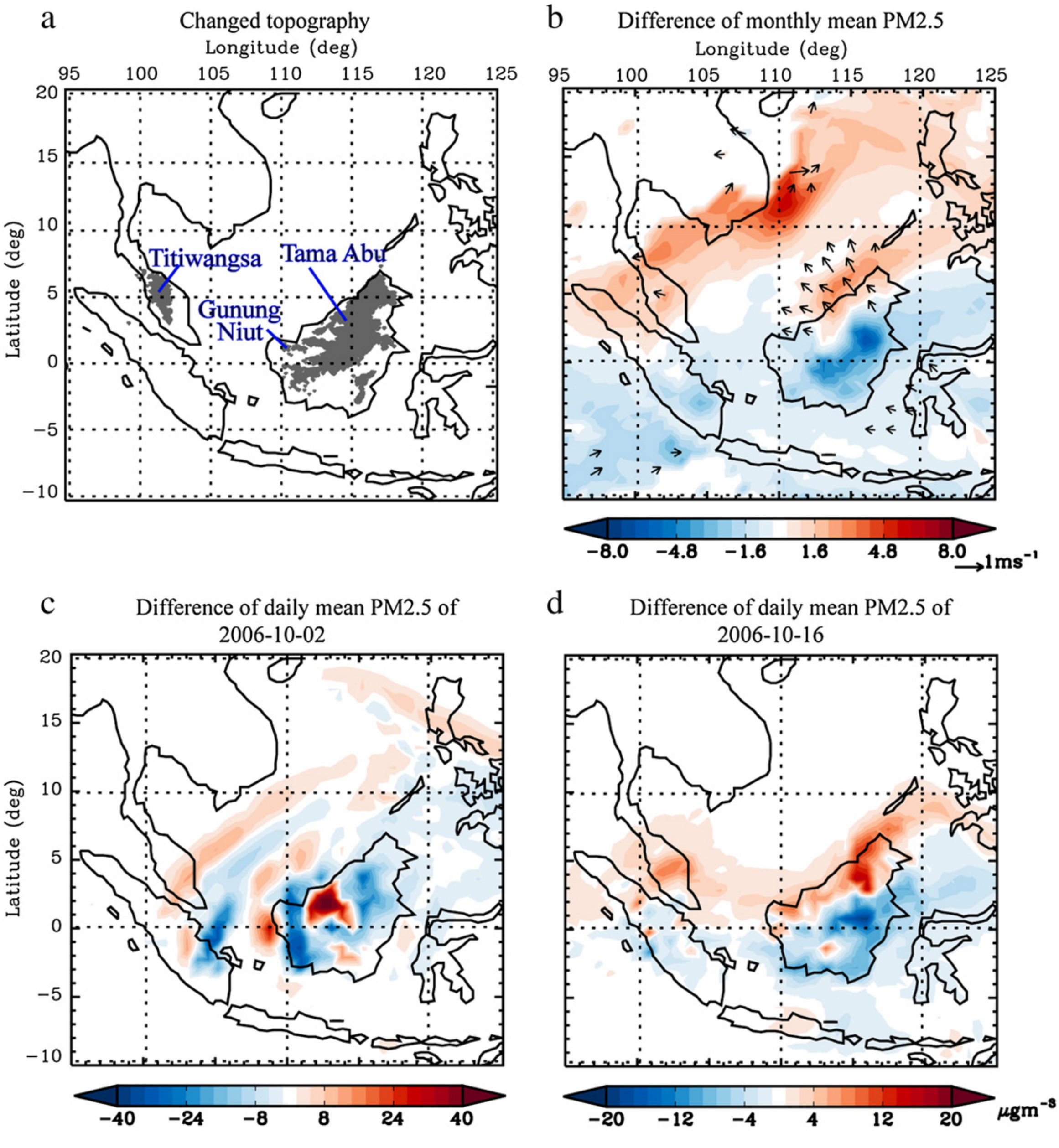


**Fig. 11.** (a) Map of shaded areas where the topography is reduced to 300 m in the simulation for studying the effect of topography on the smoke transport. Three mountain ranges, Titiwangsa, Tama Abu, and Gunung Niut, are also marked in the (a). (b) Geographical distribution of differences in averages of WRFchem simulated surface $PM_{2.5}$ mass concentration in September–October 2006 with and without reducing the topography (to 300 m as shown in (a)); also overlaid is the corresponding differences in surface wind speed. (c) and (d): same as (b) but respectively for 2 October 2006 and 16 October 2006. Note the differences in color scales for $PM_{2.5}$ in (b)–(d), and also note that difference in wind vector due to change of topography is not shown in (c) and (d).

Malaysia to Vietnam and gulf of Thailand (Fig. 11) likely because without the obstruction of the Titiwangsa mountains (that could result in less depth for vertical transport of smoke), more northern ward transport of smoke could occur from Sumatra to Peninsular Malaysia and consequently, more smoke particles are transported to the South China Sea by the southwesterly wind in the 5–10°N zone (Fig. 9a).

It is worth noting that the differences of $PM_{2.5}$ shown in Fig. 11b are for two month averages. During the episodic smoke transport, the effect of topography can result in much larger differences in the distribution of smoke particles near the surface. Fig. 11c and d show that on 2 October and 16 October 2006 (the smoke transports for these two days discussed in Sections 4.1 and 4.3 and illustrated in Figs. 6e and 3i, respectively), the differences of surface $PM_{2.5}$ due to the change of topography can be up to 40 μg m$^{-3}$ and 20 μg m$^{-3}$, respectively, suggesting the necessity of mesoscale models to resolve the topography for air quality forecasting.

## 5. Summary and discussions

Using WRFchem model in conjunction with the FLAMBE MODIS-based smoke emission inventory, we studied the smoke transport pathway in the Southeast Asian Maritime Continent during September–October 2006 when the drought associated with a moderate El Niño event caused the largest regional biomass burning outbreak since 1997. We found that temporal variation of model-simulated surface $PM_{2.5}$ dry mass concentration is in good agreement with that of the observed daily-mean $PM_{10}$ at 49 stations in Singapore and Malaysia, with correlation coefficient larger than 0.7 at most stations. The distribution of smoke particles highly manifests the complexity of meteorology in the Martine Continent, as the interplay of sea/land breeze, typhoons and storms over the subtropical western Pacific Ocean, as well as topographic effect and trade winds can be clearly seen in the model simulation of smoke transport. It is shown that the largest smoke transport episode in our study region occurred on 2 October 2006, and was associated with the typhoon Xangsane (#18 in 2006) in the subtropics that resulted in strong downdraft and dryness and thus favored the propagation of fires over central Kalimantan. The second largest event occurred in 11–18 October 2011, and is shown to be atypical because of its association with the (summer-to-winter) transitional southward movement of ITCZ.

Overall, in September–October the summer monsoon circulations prevail over the MC. As a result, the $PM_{10}$ concentrations near the surface along the Sarawak and Brunei coasts are found to be often affected by smoke transported from the biomass-burning regions in the south (Southern Kalimantan) and in the west (Sumatra). Transport of smoke from Kalimantan to Peninsular Malaysia, however, is much less frequent when compared to the transport of smoke from Peninsular Malaysia to the Sarawak coast. This is because the southeastern trade wind shifts the direction straight to the northeast, as it circulates around the Peninsular Malaysia and the west coast of Borneo. Consequently, low-level divergence can often be expected over the west coast of Borneo, which prevents the smoke from being vented to the middle and upper troposphere. Furthermore, the land/sea breeze affects the coastal meteorology on a daily basis, leading to low-level convergence of smoke aerosols over the land during the daytime, and divergence of smoke aerosols over the land during the night time. Therefore, the overall effect of land/sea breeze is to enhance the air stagnant in the vertical over the coastal land.

One exception to the above conceptual model is during the time period of the transition from the summer monsoon to the winter monsoon (such as during 11–18 October 2006). During this transition, the ITCZ moves southward, leading to (a) somewhat uniform southeasterly wind near the surface between 5 S–2.5 N, (b) low-level near surface convergence in 2.5°N–5°N associated with ITCZ, and (c) bifurcation of wind direction at 700 hPa in 0°–10°N zone (instead of the uniform westerly wind in the typical summer monsoon season). As a result, smoke particles can be transported from Kalimantan to Sumatra and then to Peninsular Malaysia, and become widely spread in the 5°S–5°N zone, reaching the southeast equatorial Indian Ocean and west equatorial Pacific Ocean, in contrast with the summer monsoon season, when smoke is transported east-northeast to the Philippines.

Common to both the boreal summer monsoon season and monsoon transition time period are: (a) the trapping of smoke aerosols within 3–4 km above the surface, (b) the important impact of the Titiwangsa Mountains on smoke transport from Sumatra to the northwest part of Peninsular Malaysia, and (c) the impact of Tama Abu Mountains on the transport of smoke from Central Kalimantan to the Malaysian Borneo coast and to the South China Sea.

One important facet of the smoke transport, as illustrated in this paper, is obtained through the use of CALIOP data to constrain the model simulation. In contrast to many previous studies that suggested that significant smoke in our study region should be uplifted to the middle troposphere and hence used the injection height of 2 km in the model simulation, CALIOP data show that smoke aerosols are often confined within 3.5 km above the surface over a wide region. This is in agreement with the studies of Tosca et al. (2011) for the Borneo area and whole MC region by Campbell et al. (2012). Consequently, we found that the smoke injection height should be set at 0.8 km in the model simulation. Furthermore, CALIOP observation also showed that within 3.5 km above the surface, smoke aerosols can still reside above the boundary layer clouds (that is ~0.5 km above the surface), which is expected to result in significant aerosol-cloud interaction and radiative heating above the clouds. Reliable simulation of 3D distribution of smoke particles, as shown in this study, therefore provides the basis for our next step to estimate smoke direct and indirect radiative forcing and quantify their feedbacks on meteorology and precipitation.

## Acknowledgment

This research is supported by NASA New Investigator Program (NNX08AQ86G) to J. Wang, NASA Atmospheric Chemistry Modeling and Analysis Program (NNX10AG60G), NASA Applied Science Program (NNX11AJ03G), and NASA Interdisciplinary Science Program. Drs. Hyer's and Reid's contributions were supported by the NRL 6.1 base program.

## References

Ackermann, I.J., Hass, H., Memmesheimer, M., Ebel, A., Binkowski, F.S., Shankar, U., 1998. Modal aerosol dynamics model for Europe: development and first applications. Atmos. Environ. 32, 2981–2999.

Barnard, J.C., Fast, J.D., Paredes-Miranda, G., Arnott, W.P., Laskin, A., 2010. Technical note: evaluation of the WRF-Chem "Aerosol chemical to aerosol optical properties" module using data from the MILAGRO campaign. Atmos. Chem. Phys. 10, 7325–7340.

Campbell, J.R., Reid, J.S., Westphal, D.L., Zhang, J., Tackett, J.L., Chew, B.N., Welton, E.J., Shimizu, A., Sugimoto, N., 2012. Characterizing aerosol particle composition and the vertical profile of extinction and linear depolarization over Southeast Asia and the Maritime Continent: the 2007–2009 view from CALIOP. Atmos. Res. http://dx.doi.org/10.1016/j.atmosres.2012.05.007.

Chang, C.-P., Wang, Z., Mcbride, J., Liu, C.-H., 2005. Annual cycle of Southeast Asia-Maritime Continent rainfall and asymmetric monsoon transition. J. Climate 18, 287–301.

Chou, M.D., Suarez, M.J., Ho, C.H., Yan, M.M.H., Lee, K.T., 1998. Parameterizations for cloud overlapping and shortwave single-scattering properties for use in general circulation and cloud ensemble models. J. Climate 11, 202–214.

Colarco, P.R., Schoebert, M.R., Doddridge, B.G., Marufu, L.T., Torres, O., Welton, E.J., 2004. Transport of smoke from Canadian forest fires to the surface near Washington, D.C.: injection height, entrainment, and optical properties. J. Geophys. Res. 109. http://dx.doi.org/10.1029/2003JD004248.

Crutzen, P.J., Andreae, M.O., 1990. Biomass burning in the tropics: impact on atmospheric chemistry and biogeochemical cycles. Science 250, 1669–1678.

Crutzen, P.J., Heidt, L.E., Krasnec, J.P., Pollock, W.H., Seiler, W., 1979. Biomass burning as a source of atmospheric gases CO, $H_2$, $N_2O$, NO, $CH_3Cl$ and COS. Nature 282, 253–256.

Davison, P.S., Roberts, D.L., Arnold, R.T., Colvile, R.N., 2004. Estimating the direct radiative forcing due to haze from the 1997 forest fires in Indonesia. J. Geophys. Res. 109. http://dx.doi.org/10.1029/2003JD004264.

Department of Environment Malaysia, 2010. http://www.doe.gov.my/portal/air-air-quality/air-quality/.

Fast, J.D., Gustafson Jr., W.I., Easter, R.C., Zaveri, R.A., Barnard, J.C., Chapman, E.G., Grell, G.A., Peckham, S.E., 2006. Evolution of ozone, particulates, and aerosol direct radiative forcing in the vicinity of Houston using a fully coupled meteorology-chemistry-aerosol model. J. Geophys. Res. 111, D21305. http://dx.doi.org/21310.21029/22005JD006721.

Field, R.D., Shen, S.S.P., 2008. Predictability of carbon emissions from biomass burning in Indonesia. J. Geophys. Res. 113, G04024. http://dx.doi.org/10.1029/2008JG000694.

Field, R.D., van der Werf, G.R., Shen, S.S.P., 2009. Human amplification of drought-induced biomass burning in Indonesia since 1960. Nat. Geosci. 2, 185–188.

Fisher, J.A., et al., 2010. Source attribution and interannual variability of Arctic pollution in spring constrained by aircraft (ARCTAS, ARCPAC) and satellite (AIRS) observations of carbon monoxide. Atmos. Chem. Phys. 10, 977–996.

Forster, C., et al., 2001. Transport of boreal fire emissions from Canada to Europe. J. Geophys. Res. 106, 22,887–22,906.

Freitas, S.R., Longo, K.M., Chatfield, R., Latham, D., Silva Dias, M.A.F., Andreae, M.O., Prins, E., Santos, J.C., Gielow, R., Carvalho Jr., J.A., 2007. Including the sub-grid scale plume rise of vegetation fires in low resolution atmospheric transport models. Atmos. Chem. Phys. 7, 3385–3398.

Giglio, L., Descloitres, J., Justice, C.O., Kaufman, Y.J., 2003. An enhanced contextual fire detection algorithm for MODIS. Remote Sens. Environ. 87, 273–282.

Giglio, L., Csiszar, I., Justice, C.O., 2006. Global distribution and seasonality of active fires as observed with the Terra and Aqua MODIS sensors. J. Geophys. Res. 111, G02016. http://dx.doi.org/10.1029/2005JG000142.

Grell, G.A., Devenyi, D., 2002. A generalized approach to parameterizing convection combining ensemble and data assimilation techniques. Geophys. Res. Lett. 29, 1693–1696.

Grell, G., Peckham, S.E., Schmitz, R., McKeen, S.A., Frost, G., Skamarock, W.C., Eder, B., 2005. Fully coupled "online" chemistry within WRF model. Atmos. Environ. 39, 6957–6975.

Guan, H., Chatfield, R.B., Freitas, S.R., Bergstrom, R.W., Longo, K.M., 2008. Modeling the effect of plume-rise on the transport of carbon monoxide over Africa with NCAR CAM. Atmos. Chem. Phys. 8, 6801–6812. http://dx.doi.org/10.5194/acp-8-6801-2008.

Hong, Song-You, Dudhia, Jimy, Chen, Shu-Hua, 2004. A revised approach to ice microphysical processes for the bulk parameterization of clouds and precipitation. Mon. Wea. Rev. 132, 103–120.

Hong, S.-Y., Noh, Y., Dudhia, J., 2006. A new vertical diffusion package with an explicit treatment of entrainment processes. Mon. Weater Rev. 134, 2318–2341.

Hyer, E.J., Chew, B.N., 2010. Aerosol transport model evaluation of an extreme smoke episode in Southeast Asia. Atmos. Environ. 44, 1422–1427.

Hyer, E.J., Allen, D.J., Kasischke, E.S., 2007. Examining injection properties of boreal forest fires using surface and satellite measurements of CO transport. J. Geophys. Res. 112, D18307. http://dx.doi.org/10.1029/2006JD008232.

Ichoku, C., Kaufman, Y.J., 2005. A method to derive smoke emission rates from MODIS fire radiative energy measurements. IEEE Trans. Geosci. Remote Sens. 11 (43), 2636–2649.

IPCC, 2007. Climate change 2007: the physical science basis. Contribution of Working Group I to the Fourth Assessment. In: Solomon, S., Qin, D., Manning, M., Chen, Z., Marquis, M., Averyt, K.B., Tignor, M., Miller, H.L. (Eds.), Report of the Intergovernmental Panel on Climate Change. Cambridge University Press, Cambridge, United Kingdom and New York, NY, USA. 996 pp.

Justice, C.O., Giglio, L., Korontzi, S., Owens, J., Morisette, J.T., Roy, D., Descloitres, J., Alleaume, S., Petitcolin, F., Kaufman, Y.J., 2002. The MODIS fire products. Remote Sens. Environ. 83, 244–262.

Kahn, R.A., Li, W.-H., Moroney, C., Diner, D.J., Martonchik, J.V., Fishbein, E., 2007. Aerosol source plume physical characteristics from space-based multiangle imaging. J. Geophys. Res. 112, D11205. http://dx.doi.org/10.1029/2006JD007647.

Kaufman, Y.J., Kleidman, R.G., King, M.D., 1998. SCAR-B fires in the tropics: properties and remote sensing from EOS-MODIS. J. Geophys. Res. 103 (31,955-931,986).

Kaufman, Y.J., Ichoku, C., Giglio, L., Korontzi, S., Chu, D.A., Hao, W.M., Li, R.R., Justice, C.O., 2003. Fire and smoke observed from the Earth Observing System MODIS instrument — products, validation, and operational use. Int. J. Remote Sens. 24, 1765–1781.

Leung, F.Y.T., et al., 2007. Impacts of enhanced biomass burning in the boreal forests in 1998 on tropospheric chemistry and the sensitivity of model results to the injection height of emissions. J. Geophys. Res. 112, D10313. http://dx.doi.org/10.1029/2006JD008132.

Levy, R.C., Remer, L.A., Mattoo, S., Vermote, E.F., Kaufman, Y.J., 2007. Second-generation operational algorithm: retrieval of aerosol properties over land from inversion of moderate resolution imaging spectroradiometer spectral reflectance. J. Geophys. Res. 112, D13211 (doi:13210.11029/12006JD007811).

Liousse, C., Penner, J.E., Chuang, C., Walton, J.J., Eddleman, H., Cachier, H., 1996. A global three-dimensional model study of carbonaceous aerosols. J. Geophys. Res. 101, 19411–19432.

Logan, J.A., Megretskaia, I., Nassar, R., Murray, L.T., Zhang, L., Bowman, K.W., Worden, H.M., Luo, M., 2008. Effects of the 2006 El Niño on tropospheric composition as revealed by data from the Tropospheric Emission Spectrometer (TES). Geophys. Res. Lett. 35, L03816 (doi:03810.01029/02007GL031698).

Mahmud, M., 2009. Mesoscale model simulation of low level equatorial winds over Borneo during the haze episode of September 1997. J. Earth Syst. Sci. 118, 295–307.

Mlawer, E.J., Taubman, S.J., Brown, P.D., Iacono, M.J., Clough, S.A., 1997. Radiative transfer for inhomogeneous atmosphere: RRTM, a validated correlated-k model for the longwave. J. Geophys. Res. 102, 16663–16682.

National Environment Agency, 2006. Annual Report of Environmental Protection Department (NEA). , pp. 27–35.

Omar, A.H., Won, J.-G., Winker, D.M., Yoon, S.-C., Dubovik, O., McCormick, M.P., 2005. Development of global aerosol models using cluster analysis of Aerosol Robotic Network (AERONET) measurements. J. Geophys. Res. 110, D10S14. http://dx.doi.org/10.1029/2004JD004874.

Ott, L., Duncan, B., Pawson, S., Colarco, P., Chin, M., Randles, C., Diehl, T., Nielsen, E., 2010. Influence of the 2006 Indonesian biomass burning aerosols on tropical dynamics studied with the GEOS-5 AGCM. J. Geophys. Res. 115, D14121 (doi:14110.11029/12009JD013181).

Randerson, J.T., Werf, G.R.v.d., Collatz, G.J., Giglio, L., Still, C.J., Kasibhatla, P., Miller, J.B., White, J.W.C., DeFries, R.S., Kasischke, E.S., 2005. Fire emissions from $C_3$ and $C_4$ vegetation and their influence on interannual variability of atmospheric $CO_2$ and $d^{13}CO_2$. Global Biogeochem. Cycles 19, GB2019 (doi:2010.1029/2004GB002366).

Reid, J.S., et al., 2013. Observing and understanding the Southeast Asian aerosol system by remote sensing: An initial review and analysis for the Seven Southeast Asian Studies (7SEAS) program. Atmos. Res. 122, 403–468.

Reid, J.S., Prins, E.M., Westphal, D.L., Schmidt, C.C., Richardson, K.A., Christopher, S.A., Eck, T.F., Reid, E.A., Curtis, C.A., Hoffman, J.P., 2004. Real-time monitoring of South American smoke particle emissions and transport using a coupled remote sensing/box-model approach. Geophys. Res. Lett. 31, L06107 (doi:06110.01029/02003GL018845).

Reid, J.S., Koppmann, R., Eck, T.F., Eleutrio, D.P., 2005. A review of biomass burning emissions part II: intensive physical properties of biomass burning particles. Atmos. Chem. Phys 5 (3), 799–825.

Reid, J., et al., 2009. Global monitoring and forecasting of biomass-burning smoke: description and lessons from the Fire Locating and Modeling of Burning Emissions (FLAMBE) program. IEEE J. Spec. Top. Appl. Earth Observations Remote Sens. (J-STARS) 2, 144–162.

Reid, J.S., Xian, P., Hyer, E.J., Flatau, M.K., Ramirez, E.M., Turk, F.J., Sampson, C.R., Zhang, C., Fukada, E.M., Maloney, E.D., 2011. Multi-scale meteorological

conceptual model of observed active fire hotspot activity and smoke optical depth in the Maritime Continent. Atmos. Chem. Phys. Discuss. 11, 21091–21170. http://dx.doi.org/10.5194/acpd-11-21091-2011.
Schell, B., Ackermann, I.J., Hass, H., Binkowski, F.S., Ebel, A., 2001. Modeling the formation of secondary organic aerosol within a comprehensive air quality model. J. Geophys. Res. 106 (22) (28,275-228,293).
Seiler, W., Crutzen, P.J., 1980. Estimates of gross and net fluxes of carbon between the biosphere and the atmosphere from biomass burning. Clim. Chang. 2, 207–247.
Sessions, W.R., Fuelberg, H.E., Kahn, R.A., Winker, D.M., 2011. An investigation of methods for injecting emissions from boreal wildfires using WRF-Chem during ARCTAS. Atmos. Chem. Phys. 11, 5719–5744. http://dx.doi.org/10.5194/acp-11-5719-2011, 2011.
Stockwell, W.R., Middleton, P., Chang, J.S., Tang, X., 1990. The second generation regional acid deposition model chemical mechanism for regional air quality modeling. J. Geophys. Res. 95 (16,343–316,367).
Swap, R.J., Annegarn, H.J., Suttles, J.T., King, M.D., Platnick, S., Privette, J.L., Scholes, R.J., 2003. Africa burning: a thematic analysis of the Southern African Regional Science Initiative (SAFARI 2000). J. Geophys. Res. 108 (13). http://dx.doi.org/10.1029/2003JD003747.
Thampi, B.V., Rajeev, K., Parameswaran, K., Mishra, M.K., 2009. Spatial distribution of the Southeast Asian smoke plume over the Indian Ocean and its radiative heating in the atmosphere during the major fire event of 2006. Geophys. Res. Lett. 36, L16808 (doi:16810.11029/12009GL039316).
Tosca, M.G., Randerson, J.T., Zender, C.S., Nelson, D.L., Diner, D.J., Logan, J.A., 2011. Dynamics of fire plumes and smoke clouds associated with peat and deforestation fires in Indonesia. J. Geophys. Res. 116, D08207. http://dx.doi.org/10.1029/2010JD015148.
Val Martin, M., Logan, J.A., Kahn, R., Leung, F.-Y., Nelson, D., Diner, D., 2010. Smoke injection heights from fires in North America: analysis of five years of satellite observations. Atmos. Chem. Phys. 10, 1491–1510.
van der Werf, G.R., Randerson, J.T., Giglio, L., Gobron, N., Dolman, A.J., 2008. Climate controls on the variability of fires in the tropics and subtropics. Global Biogeochem. Cycles 22 (3).
Wang, J., Christopher, S.A., 2006. Mesoscale modeling of Central American smoke transport to the United States, Part II, smoke radiative impact on regional surface energy budget and boundary layer process. J. Geophys. Res. 111, D14S92. http://dx.doi.org/10.1029/2005JD006416.
Wang, J., Christopher, S.A., Nair, U.S., Reid, J.S., Prins, E.M., Szykman, J., Hand, J.L., 2006. Mesoscale modeling of Central American smoke transport to the United States, part I: “top-down” assessment of emission strength and diurnal variation impact. J. Geophys. Res. 111, D05S17. http://dx.doi.org/10.1029/2005jd006720.
Westphal, D.L., Toon, O.B., 1991. Simulations of Microphysical, radiative, and dynamical processes in a continental-scale forest fire smoke plume. J. Geophys. Res. 96 (D12), 22,379–22,400. http://dx.doi.org/10.1029/91JD01956.
Winker, D.M., Vaughan, M.A., Omar, A., Hu, Y., Powell, K.A., Liu, Z., Hunt, W.H., Young, S.A., 2009. Overview of the CALIPSO mission and CALIOP data processing algorithms. J. Oceanogr. Atmos. Meas. 26, 2310–2323.
Winker, D.M., et al., 2010. The CALIPSO mission: a global 3D view of aerosols and clouds. Bull. Am. Meteorol. Soc. 91, 1211–1229.
Xian, P., Reid, J.S., Atwood, S.A., Johnson, R.S., Hyer, E.J., Westphal, D.L., Sessions, W., 2012. Smoke aerosol transport patterns over the maritime continent. Atmos. Res. http://dx.doi.org/10.1016/j.atmosres.2012.05.006.
Zhao, C., Liu, X., Leung, L.R., Johnson, B., McFarlane, S.A., Gustafson Jr., W.I., Fast, J.D., Easter, R., 2010. The spatial distribution of mineral dust and its shortwave radiative forcing over North Africa: modeling sensitivities to dust emissions and aerosol size treatments. Atmos. Chem. Phys. 10, 8821–8838.